# Creation, detection, and decoherence of macroscopic quantum superposition states in double-well Bose-Einstein condensates

Y. P. Huang and M. G. Moore
*Department of Physics & Astronomy, Ohio University, Athens, Ohio 45701, USA*
(Received 24 August 2005; published 7 February 2006)

We study the possibility of creating many-particle macroscopic quantum superposition (Schrödinger cat)–like states by using a Feshbach resonance to reverse the sign of the scattering length of a Bose-Einstein condensate trapped in a double-well potential. To address the issue of the experimental verification of coherence in the catlike state, we study the revival of the initial condensate state in the presence of environmentally induced decoherence. As a source of decoherence, we consider the interaction between the atoms and the electromagnetic vacuum, due to the polarization induced by an incident laser field. We find that the resulting decoherence is directly related to the rate at which spontaneously scattered photons carry away sufficient information to distinguish between the two atom distributions which make-up the cat state. We show that for a "perfect" cat state, a single scattered photon will bring about a collapse of the superposition, while a less-than-perfect catlike state can survive multiple scatterings before the collapse occurs. In addition, we study the dephasing effect of atom-atom collisions on the catlike states.

DOI: 10.1103/PhysRevA.73.023606 PACS number(s): 03.75.Gg, 32.80.Lg, 03.75.Lm

## I. INTRODUCTION

Quantum degenerate gases of bosonic and/or fermionic atoms have proven very useful tools in the exploration of low-temperature many-body quantum physics. In this area of research, the initial Bose-Einstein condensate (BEC) or degenerate Fermi gas (DFG) serves primarily as a well-defined starting point for the generation of more exotic highly correlated and/or entangled many-body states. The most profound recent experimental demonstrations of this approach include the observations of the superfluid to Mott-insulator transition in an optical lattice and the cross-over to a "fermionized" Tonks-Girardeau gas under quasi-one-dimensional confinement [1–5]. In addition, there has been significant progress towards observing the BEC to BCS cross-over in a two-component gas of Fermionic atoms [6,7], and efforts are underway to observe the cross-over from a vortex lattice to a nontrivial entangled many-body state in the ground state of a rapidly rotating BEC [8,9].

In the first of the aforementioned experiments, a reversible change from a superfluid to a Mott-insulator state was observed when crossing from the tunneling-dominated to the collision-dominated regime for atoms trapped in a lattice potential with repulsive atom-atom interactions. The analogous transition for the case of attractive interactions involves the crossover from a superfluid into a macroscopic quantum superposition state (often described as a Schrödinger "cat" state), where the atomic population collapses into a single lattice site, with the true ground state being a symmetric superposition over all possible lattice sites as the final occupied site. In addition to providing fundamental insights into the nature of the transition from the quantum to the classical descriptions of reality, such states may have important applications in precision measurement [10] and quantum information processing.

In this paper we investigate theoretically the possibility of using a BEC trapped in a double-well potiential to generate highly entangled Schrödinger cat-type state, which can be viewed as a realization [11] of the two-site Bose-Hubbard model with attractive interactions. We address important issues such as detection of catlike states and the effects of photon-scattering-induced decoherence which occurs when far-off-resonant laser light is used for trapping and/or probing the cat states.

Interest in Schrödinger catlike states, loosely defined as quantum superpositions of macroscopically distinguishable many-body states, goes back to the earliest days of quantum mechanics. In 1935, in oder to demonstrate the limitations inherent in using quantum mechanics to describe everyday phenomena, Erwin Schrödinger proposed a experiment in the macroscopic state of a cat is entangled with that of an unstable nuclei, allowing the cat to enter a coherent superposition of being dead and alive [12]. Such states were thought at the time to be logically untenable, although today we might consider only that they would not be observed due to rapid environmentally induced decoherence [13]. To this day, this famous gedanken experiment illustrates the fundamental difficulties inherent postulating a well-defined boundary between a "classical" level of reality and an underlying level governed by quantum mechanics, one of the fundamental open questions in quantum theory.

Many of the early gedanken experiments, whose consideration led to the earliest understanding of quantum mechanics, are now being transformed into laboratory realities. One such effort has been the ongoing quest for Schrödinger–catlike states, with the most striking experimental results to date being the observation of a superposition between clockwise and counter-clock-wise currents in a superconducting quantum interference device [14] and the observation of double-slit diffraction for massive $C_{60}$ molecules [15]. Additional efforts include work in trapped ions at low temeperature [16,17], nanoscale magnets [18], and superconductors [19–21]. This progress is generating a deeper insight into the meaning of quantum theory, as well as potential applications

 ©2006 The American Physical Society

in the fields of precision measurement and quantum information processing. Even with the current rapid rate of progress, the quest to obtain and utilize large catlike states remains a serious experimental challenge, due primarily to the presumed scaling of fragility (with respect to environmentally induced decoherence) with a number of particles. For most appliciations, the utility of the cat state increases with the particle number [22,23], so there is a strong need to find systems in which such maximally entangled states of large numbers of particles can be generated without rapid collapse due to decoherence.

An atomic BEC [24–26] may be such a system, as its large degree of spatial and temporal coherence is well established by experiment [27]. The bimodal BEC, which is constructed by isolating a pair of weakly coupled atomic-field modes, is one of the simplest quantum systems used in the study of entanglement physics and has, therefore, been the subject of extensive theoretical study [28,29]. In this system, $N$ bosons are restricted to occupy one of two modes, and entanglement is established via two-body interactions between the bosons. For the case of an atomic BEC, the two modes can either be two potential wells spatially separated by a potential barrier (so-called double-well BEC's) [30,31] or two spatially overlapping modes in different hyperfine states [32,33]. In addition, a recent paper proposes an analogous system in which a double-well "potential" in momentum space, formed from the band structure in a lattice potential, can be used to create cat states involving two momentum states [34].

The quantum ground state of the bosonic double-well system has been studied for the case of repulsive interactions in the context of the superfluid to Mott-insulator transition [35], as well as for the case of attractive interactions. For the latter, it has been shown under certain conditions a Schrödinger catlike macroscopic superposition state can be generated [36,37]. In this catlike many-body state, a large number of atoms are collectively either in one mode or in another. The dynamics of the bimodal system has also been investigated, both via a mean-field approach and a full many-body treatment within the two-mode approximation. In the mean-field treatment, the dynamic evolution is treated as a Bose-Josephson junction, which is complementary to that of a superconductor tunnel junction [38,39]. This treatment predicts a degenerate ground state, corresponding to all the amplitude in one well or the other, but is not capable of predicting the dynamical evolution of catlike states, as these states lie outside of the domain of the mean-field theory. In the two-mode many-body treatment, the many-particle catlike state is predicted to arise during the dynamical evolution of an initial minimally entangled condensate state in the presence of repulsive interactions [31,32], but with the sign of the tunneling coefficient reversed by imprinting a $\pi$-phase shift onto one well. In this paper, we propose that such cat states can be realized for the case of an atomic BEC trapped in a double-well potential by employing a magnetic Feshbach resonance to tune the atomic interaction from repulsive to attractive [40,41]. It is found that for suitable parameters, the initial state will evolve into a catlike state after a certain period of time, and then it will revive back to the initial state.

Despite these theoretical advances, there remain many challenges, some of which we address in the present paper. One challenge is the problem of experimental verification of the coherence between macroscopically distinguishable states, which is related to the challenge of understanding the role played by environmentally induced decoherence in collapsing the cat state onto a statistical mixture of the two macroscopically distinguishable possibilities. In this paper we focus in detail on the decoherence which will occur if laser light is used for trapping and/or probing of the cat states. In addition the influence of atom-atom interactions on the proposed detection scheme is studied in some detail. As suggested in [32], we show the revival of the initial state can be used as an unambiguous signal that the supposed cat state is indeed a coherent macroscopic superposition, as opposed to an incoherent mixture. We also demonstrate, however, that collisional dephasing can mask the revival without a true loss of coherence.

The effects of decoherence on these catlike states have primarily been discussed for the case of coupling to the thermal cloud of noncondensate atoms [32,42,43]. We note, however, that these authors treat the noncondensate fraction as a Markovian reservoir, which implies an infinitely short memory (relative to condensate evolution times) for correlations between the condensate and noncondensate terms. We question this assumption, primarily due to the fact that the noncondensate fraction typically has a very low temperature and density. In addition, the noncondensate atoms are trapped inside the condensate volume by the trapping potential, thus there is no irreversible loss of information due to propagation of the entangled atoms outside of the system volume. Hence, we suspect that a non-Markovian treatment is necessary to accurately evaluate the thermal-cloud-induced decoherence. However, modeling this is a difficult task that we do not address at present. Instead, we assume that this effect is negligible and concentrate primarily on an analysis of a new source of decoherence: that due to spontaneous scattering of far-off-resonant photons from laser fields which we presume are used in either the trapping and/or probing of the system. In this case, the correlation time of the reservoir is governed by the irreversible loss of the scattered photons from the system volume at the extremely fast rate of $L/c$ where $L$ is the atomic mode size and $c$ is the speed of light. Hence, the Markov approximation works extremely well for describing the physics of photon scattering. As is well known, this approach leads to effective interactions as well as decoherence, effects which include induced dipole-dipole interactions and collective spontaneous emission (superradiance) in the atomic ensemble [44–46].

When analyzing the effects of environmentally induced decoherence we are interested in answering two basic questions: (1) What limitations are imposed on the ability to create cat states, and revive the initial condensate states by the presence of decoherence? and (2) how long can one "hold" the cat state by decreasing the tunnel coupling to zero, without collapse of the cat state onto a mixed state?. The second question is raised in anticipation of applications in precision measurement and quantum information processing where the cat state is operated on and/or held ready for future operations during a complicated protocol. We therefore need to determine the lifetime of the cat states in the presence of decoherence, as well as the effect of decoherence on the

dynamical evolution from the initial state into the cat state.

The organization of this paper is as follows. In Sec. II the model of bimodal BEC in double-well systems is introduced and the cat states in such a system are defined; in Sec. III two schemes of creating cat states are discussed: adiabatic evolution of the ground state and and dynamical evolution of a nonstationary state. We demonstrate that the former is experimental unfeasible due to the fact that the end state is nearly degenerate with the first-excited state. We then propose generating a catlike state through dynamic evolution following a sudden flipping of the sign of the atomic interaction, accomplished via Feshbach resonance. In Sec. IV the method of detecting the cat state via revival of the initial state is discussed in detail. In Sec. V we investigate the decoherence of cat states and a master equation is derived for the laser-induced decoherence. In addition, the lifetime of cat states in the presence of laser fields is determined. In Sec. VI the dephasing effects due to the nonlinear two-body interaction is studied. And finally, we briefly summarize our results in Sec. VII.

## II. THE MODEL

Our proposed scheme involves loading a BEC into a double-well potential and then employing a Feschbach resonance to vary the atomic scattering length in order to produce a Schrödinger catlike state. For the present we consider only the case of a spatial double-well potential. However, an analogous system can be formed by using a Raman scheme to couple two hyperfine states in a spinor BEC. The primary difference between this model and the double-well system lies in the presence of collisional interactions between the two modes, due to the spatial overlap of the hyperfine modes. Our current model neglects these collisions, as they are negligible for the case of well-separated potential minima. Most of our results should apply to both systems, however, the effects of intermode collisions will be considered in future work.

We begin our analysis from the usual many-body Hamiltonian describing atomic BEC,

$$\hat{H} = \int d^3r\, \hat{\Psi}^\dagger(\mathbf{r})\left[-\frac{\hbar^2}{2m}\nabla^2 + V_{trap}(\mathbf{r})\right]\hat{\Psi}(\mathbf{r}) + \frac{U_0}{2}\int d^3r\, \hat{\Psi}^\dagger(\mathbf{r})\hat{\Psi}^\dagger(\mathbf{r})\hat{\Psi}(\mathbf{r})\hat{\Psi}(\mathbf{r}), \tag{1}$$

where $m$ is the atomic mass, $V_{trap}$ is the trapping potential, and $\hat{\Psi}$ is the annihilate field operator for atoms in the Heisenberg picture. The two-body interaction strength is given by $U_0 = 4\pi a\hbar^2/m$, with $a$ denoting the $s$-wave scattering length. In our model, the BEC is assumed to occupy a symmetric double-well potential.

The single-atom ground state and first excited state in this system we denote as $\psi_s(\mathbf{r})$ and $\psi_a(\mathbf{r})$, respectively, where $\psi_s(\mathbf{r})$ is symmetric with respect to the double-well symmetry and $\psi_a(\mathbf{r})$ is antisymmetric. We denote the energy gap between these states as $\hbar\tau$, which is typically much smaller than the gap between the first and second excited states. Because of this gap, we assume throughout that the atomic population is restricted to these two modes alone. It is convenient to introduce two localized states $\psi_L$, $\psi_R$ [47],

$$\psi_L(\mathbf{r}) = \frac{1}{\sqrt{2}}[\psi_s(\mathbf{r}) + \psi_a(\mathbf{r})],$$

$$\psi_R(\mathbf{r}) = \frac{1}{\sqrt{2}}[\psi_s(\mathbf{r}) - \psi_a(\mathbf{r})]. \tag{2}$$

Expanding the field operator $\hat{\Psi}(\mathbf{r})$ onto these two modes gives

$$\hat{\Psi}(\mathbf{r},t) = \hat{c}_L(t)\psi_L(\mathbf{r}) + \hat{c}_R(t)\psi_R(\mathbf{r}), \tag{3}$$

where $\hat{c}_L$ and $\hat{c}_R$ are bosonic atom-annihilation operators for the left and right modes, respectively. Inserting this expansion back into the many-body Hamiltonian (1), one recovers the two-mode version of the Bose-Hubbard model

$$\hat{H} = -\hbar\tau(\hat{c}_L^\dagger\hat{c}_R + \hat{c}_R^\dagger\hat{c}_L) + \hbar g(\hat{c}_L^{\dagger 2}\hat{c}_L^2 + \hat{c}_R^{\dagger 2}\hat{c}_R^2). \tag{4}$$

In deriving this expression, we have implicitly assumed that atomic collisions in the overlapping region of the two modes are negilibile, valid under the assumption that the two modes are well separated. The intrawell two-body interaction strength is indicated by $g$, where $g = U_0/2\hbar\int d^3r|\psi_L(\mathbf{r})|^4$. The interwell tunneling rate $\tau$ is determined by the single-atom energy gap between the first excited and the ground state. Note that in the deriving of the bimodal Hamiltonian (4), the wave function for each mode is assumed to be independent of particle number in the trap, and the terms proportional to the total atom number operator have been dropped, as the atom number is assumed to be a conserved quantity.

The quantum state of this bimodal system can be expessed as a superposition of Fock states $|n\rangle$ [29]

$$|\hat{\Psi}\rangle = \sum_{n=-N/2}^{N/2} c_n|n\rangle, \tag{5}$$

where

$$|n\rangle = \frac{(c_L^\dagger)^{N/2+n}(c_R^\dagger)^{N/2-n}}{\sqrt{(N/2+n)!(N/2-n)!}}|0\rangle. \tag{6}$$

Here, $N$ is the total number of atoms in the condensate which for convenience we take as a even number, and $n$ denotes the half number difference between the two modes. The two corresponding operators are

$$\hat{N} = \hat{c}_L^\dagger\hat{c}_L + \hat{c}_R^\dagger\hat{c}_R,$$

$$\hat{n} = \tfrac{1}{2}(\hat{c}_L^\dagger\hat{c}_L - \hat{c}_R^\dagger\hat{c}_R). \tag{7}$$

In this representation, the conventional Schrödinger cat state is defined as

$$|\mathrm{cat}\rangle = \frac{1}{\sqrt{2}}(|N/2\rangle + |-N/2\rangle), \tag{8}$$

where the $N$ particles have equal probability to be all in the left or all in the right mode. This cat state is an ideal maxi-

mally entangled state, however it will be difficult to create such a state in this bimodal system. Instead, a more experimental accessible catlike state is one containing two well-separated wave packets in the distribution of $c_n$. For example, a typical catlike state can be of the form

$$c_n \propto e^{(n-n_0)^2/2\sigma^2} + e^{(n+n_0)^2/2\sigma^2}, \tag{9}$$

with $n_0 > \sigma$.

In the present bimodal system the class of catlike states is more general than the Gaussian form (9). Instead, a useful catlike state only needs to satisfy two conditions: (i) the probability distribution in Fock space should be approximately symmetric; and (ii) the two wave packets should be well separated in order to correspond to macroscopically distinguishable states. In the present model, condition (i) is satisfied provided the initial state is symmetric, due to the symmetry of Hamiltonian (4). As we will see in Sec. V, decoherence may break this symmetry. Nonetheless, to distinguish catlike states from non-cat states, it is convenient to introduce a projection operator $\hat{P}_{cat}$

$$\hat{P}_{cat} = \sum_{n=n_c}^{N/2} (|n\rangle\langle n| + |-n\rangle\langle -n|). \tag{10}$$

This operator acts as a filter which picks up cat states with a minimum wave-packet separation of $2n_c$. And the expectation value $\langle \hat{P}_{cat} \rangle$ can be an efficient way to determine whether a state is catlike. It is straightforward to see that for a catlike state we will have $\langle \hat{P}_{cat} \rangle \approx 1$, whereas for a non-cat state the trace will be noticeably less than unity.

## III. GENERATION OF CAT STATES

As shown both theoretically and experimentally, the *s*-wave scattering length of cold atoms can be modulated by applying a varied magnetic field. In the vicinity of a Feshbach resonance, it takes the form

$$a = a_0 \left( 1 - \frac{\Delta B}{B - B_0} \right), \tag{11}$$

where $a_0$ is the background value, $B_0$ is the resonant value of the magnetic field, and $\Delta B$ is the width of the resonance. By tuning the magnetic field $B$, the scattering length $a$ can be efficiently tuned in an adequate range based on the Feshbach resonance, as demonstrated in recent experiments. Thus, the two-body interaction term $g$ in Hamiltonian (4), which is determined by the scattering length $a$, is implicitly assumed to be an arbitrary adjustable number.

Before discussing the methods of generating cat states, we note that attractive BEC's can collapse due to instability, as has been demonstrated in experiments [48]. A trapped BEC, however, can be stable against collapse under the condition of low atomic density [49]. In terms of the BEC atom number $N$, the attractive interaction strength $g$ and the energy gap between the first excited state and ground state $\Delta\omega$, the stability condition can be written as

$$N < \frac{\Delta\omega}{|g|}. \tag{12}$$

In the present discussion one can increase the energy gap between the ground and excited state by adjusting the trapping potential, and in this way, we can ensure our system will not collapse when the sign of the scattering length is switched from positive to negative.

### A. Adiabatic evolution

In this subsection, we begin by briefly discussing the possibility of creating cat states via adiabatic manipulation of the many-body ground state [36,37], achieved by a continuous variation of the interaction strength $g$ from a positive to a negative value. In order to better understand the adiabatic evolution of the ground state, we first examine the ground state under certain parameter values for which it can be determined exactly.

The first case we consider is that of zero tunneling, in which case the bimodal Hamiltonian (4) can be reduced to

$$\hat{H} = 2\hbar g \hat{n}^2. \tag{13}$$

The ground state of this Hamiltonian is determined solely by the parameter $g$. For $g > 0$, corresponding to repulsive interactions, the ground state will be $|0\rangle$ in our number-difference representation (6), i.e., an insulator state. While in the case of $g < 0$, the ground state is doubly degenerate, corresponding to any arbitrary superposition of the two extreme states $|N/2\rangle$ and $|-N/2\rangle$, and its orthogonal counterpart. These states can be written as

$$\frac{1}{\sqrt{\alpha^2 + \beta^2}} (\alpha |N/2\rangle + \beta |-N/2\rangle \ , \tag{14}$$

with $\alpha, \beta$ being arbitrary complex numbers. Note when $\alpha = \beta$, one recovers the Schrödinger cat state (8).

In the other extreme case, if there is no atomic interaction but only the tunneling term, the ground state of Hamiltonian (4) becomes the two-site analog of the superfluid phase [29]

$$|g\rangle = 2^{-N/2} \sum_{-N/2}^{N/2} \sqrt{\binom{N}{n}} |n\rangle, \tag{15}$$

which is a binomial distribution of Fock states, and thus approximately Gaussian when $N$ is a large number. Henceforth, we shall refer to this class of states as a "coherent state," meaning that each atom is in a coherent superposition of both modes and there are no atom-atom correlations or many-body entanglements.

The more general ground state of our model, with the presence of both collisions and tunneling, can be understood as a smooth cross-over between these two extremes. First, under the condition of a repulsive atomic interaction, the ground states of this system can be well approximated by a single Gaussian-like distribution of $c_n$ peaked at $n=0$

$$c_n \propto e^{-n^2/(2\sigma^2)}, \tag{16}$$

where the relative atom number dispersion $\sigma$ is obtained by minimizing by the mean energy of the Hamiltonian. Second,

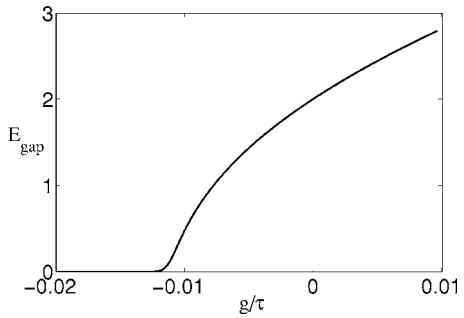


FIG. 1. The energy gap $E_{gap}$ as a function of ratio $g/\tau$. Here, $E_{gap}=E_1-E_0$, with $E_0, E_1$ being the eigenenergies of the ground and first excited state, respectively.

under the condition of the attractive two-body interaction, the ground state of this system will be split into two separated wave packets. Thus instead of (16), a good approximation of this state turns out to be a superposition of two Gaussian distributions (9) [37], where again the minima center $n_0$ and spread width $\sigma$ are obtained by minimizing the mean energy. For repulsive atomic interactions, the energy minima is found at $n_0=0$, which indicates that the atom number distribution does not split. For attractive interactions, $n_0 \neq 0$, and under the condition of $n_0 > \sigma$, the wave packet of ground states will split and become a superposition of two well-separated components, i.e., it becomes a catlike state (9). Note for this state, the relative phase for any Fock basis pair $|n\rangle$ and $|-n\rangle$ is zero.

Based on these considerations, it is of theoretical interest to determine whether or not the Schrödinger cat state in this bimodal BEC system can be generated by an adiabatic process [36,37]. As a basic scheme, the system would be first prepared in the many-body ground state with positive $g$, corresponding to a coherent state centered at $n=0$. Then by slowly tuning $g$ to be negative, the distribution will split and finally end up with a Schrödinger catlike state under the condition of $n_0 > \sigma$.

There is a significant difficulty with this proposal, however, in that when the two wave packets in Fock space are well separated, the ground state, which is the desired cat state, is nearly degenerate with the first excited state, as shown in Fig. 1. It is observed that when $g$ is positive, there is a relatively large energy gap between the ground and first excited states. Then as $g$ decreases, the energy gap decreases so that at some point the energy gap becomes exponentially small. In Fig. 2, we show the corresponding wave functions of the ground and first excited states $c(n)$ with different ratios $g/\tau$. It is clear that the ground state does not evolve into a cat state until the bimodal system enters the degenerate regime. In the degenerate regime, any small perturbation can mix the two states. As the first excited state is nearly identical with the ground state, but with a $\pi$ phase shift between the left and right wave packets, an arbitrary superposition of these two states could easily correspond to a localized state, which is equivalent to a collapse of the Schrödinger cat wave function. Strictly speaking, this degeneracy implies that to adiabatically create the cat state, the process requires an exponentially long time. Thus experimental realization appears impractical, particularly when considering the inevitable exposure of the system to noise.

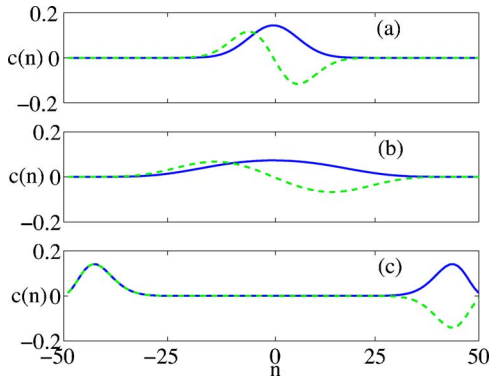


FIG. 2. (Color online) The wave packet $c(n)$ of the ground state (solid line) and first excited sate (dashed line) with (a) $g/\tau=0.01$, (b) $g/\tau=-0.01$, and (c) $g/\tau=-0.02$, respectively.

### B. Dynamic evolution

An alternate approach to a Schrödinger cat state, based on dynamical evolution, has been studied for some time [32]. In this subestion, we show that it is feasible to dynamically create the cat state from a coherent state by using a Feshbach resonance to make a sudden change in the scattering length. Our proposed scheme is as follows. First, our system is prepared in the ground state with repulsive interactions and strong tunneling between wells. This could be accomplished, e.g., by preparing a BEC in a single well, and then adiabatically raising a barrier to divide the well into two equal parts. Note here, the quantum state of this system is coherent in the sense that each atom in the condensate is independently in a superposition of the two localized states. The interaction parameters in this initial stage are chosen to satisfy $g=\tau/0.9N$ as this will lead to the optimal catlike state attainable in this scheme [47]. Once this state is established, the Feshbach resonance is used to achieve a sudden switch of the sign of the scattering length, i.e., we go from $g=\tau/0.9N$ to $g=-\tau/0.9N$. In order to avoid the collapse of the condensate when scattering length $a$ becomes negative, the amplitude of atomic interaction $g$ should be small. At this point, with tunneling still on, the initial state is no longer an eigenstate, thus it will start a dynamic evolution under the new Hamilton.

The evolution of the initial coherent state after the change in the sign of $g$ is shown in Fig. 3. It is seen that catlike states are formed periodically, and between two consequent cat states the system approximately revives back to the initial coherent state. We have determined that the best cat state appears at time $t=14.5/\tau$, which corresponds to the final state shown in Fig. 3. Once the cat state is formed, one needs to freeze the dynamic evolution at a time when the system is in the cat state. This can be accomplished by suddenly rising the barrier between the two modes to reduce the tunneling coeffient $\tau$ to zero.

Since the present proposal is based on a dynamic procedure, predicting the time when the cat state is produced $t_{cat}$ is of critical importance. Due to the imposed constraint $\tau=0.9Ng$, which is necessary to obtain an optimal cat state, $t_{cat}$ can be expressed solely in terms of the tunneling rate $\tau$ as

$$t_{cat}=\frac{\kappa}{\tau}, \tag{17}$$

where $\kappa$ is determined from our simulations to be $\kappa \approx 14.5$.

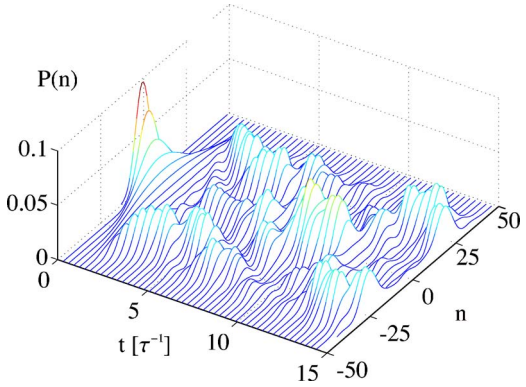


FIG. 3. (Color online) Evolution of the probability distribution $P(n)=|c_n|^2$ versus $n$, with $N=100$. At $t=0$, the initial state is taken as the ground state with $g=\tau/(0.9N)$. Then, the two-body interaction is suddenly switched to the negative value $g=-\tau/(0.9N)$. The wave packet then evolves, where it shows a collapse and revival process. It is seen that, at a time of $t=14.5/\tau$, a well peaked cat state is obtained with two well-separated wave packet centers at around $n=25,75$, respectively.

In Fig. 4, we show the dynamics evolution of projection operator $P_{cat}$. Again, it is shown that the optimum catlike state forms at around $t=t_{cat}=14.5/\tau$ and reappears again at intervals of $t=10/\tau$. It is also noticed that between each cat state, there are valleys of $P_{cat}$, which correspond to revivals of the initial coherent state.

It is also of interest to study the relative phases between the Fock states in the catlike state generated in this manner. The symmetry between left and right modes is automatically guaranteed in our model since our system Hamiltonian (4) and our initial state are both symmetric. In Fig. 5, we see that the phase of created cat state is exactly symmetric around $n=0$. In addition, we see that the phase flattens somewhat in the vicinity of $n=\pm 25$, where the peaks in the probability are located.

We have claimed that imposing the condition $\tau=0.9Ng$ is necessary to produce the optimal cat state. It is worth pointing out that with other choices, left-right symmetric states can be created, but these are neither well separated nor double peaked. This is shown in Fig. 6, where we plot the

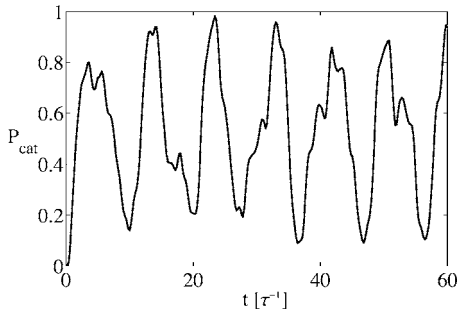


FIG. 4. Time evolution of the expectation value of the projector $P_{cat}$ with system parameters chosen as in Fig. 3 and a filtering window of width $n_c=15$. A well peaked cat state is created at $t=14.5/\tau, 24/\tau, 34/\tau\cdots$. Note the $P_{cat}$ reaches a minimum at $t\approx 10/\tau, 20/\tau, 30/\tau\cdots$, which corresponds to the revival of the initial coherent state.

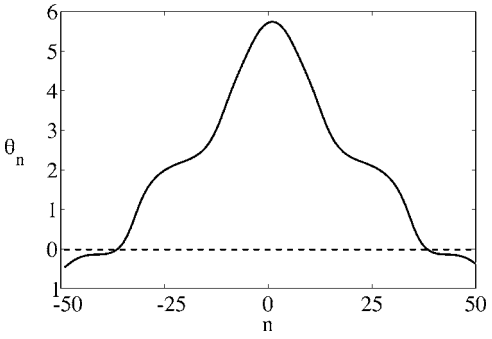


FIG. 5. Phase distribution of the created Schrödinger cat state in Fock space. The $y$ axis is the phase $\theta_n=\arg(c_n)$.

expectation value of the projector $P_{cat}$ versus $\delta_g$, where we have taken $g=\tau/0.9N(1+\delta_g)$. In this figure, we see that the catlike state is only created in the vicinity of $\delta_g=0$ with an uncertainty of approximately $\pm 5\%$. That means to create a cat state in the present system, a precise control of the atomic interaction $g$ and tunneling rate $\tau$ is required. It is important to note that in generating Fig. 6 we have varied the evolution time $t_{cat}$ for each parameter choice, in order to maximize the projection $P_{cat}$. Thus Fig. 6 can be interpreted as verifying the conditions $g=\tau/0.9N$ and $t_{cat}=14.5/\tau$.

Up to now we have only considered the ideal situation where the initial state is exactly prepared in the ground state and the atomic scattering length can be tuned in a precise way. This may not necessarily hold true under experimental conditions, where random fluctuations in system parameters may affect the formation of the cat state. Here, to test the susceptability of the present proposal to such fluctuations, we study the dependence of the final cat state on the precision of the initial state by adding random noise to the exact ground state. Thus, the initial state becomes $c_n+\delta_r$. The random noise $\delta_r$ is a complex with an amplitude drawn from a Gaussian distribution, and a completely random phase. The probability distributions for the amplitude and phase are therefore

$$P(|\delta_r|) = \frac{1}{\sqrt{\pi}\sigma_r} e^{-|\delta_r|^2/\sigma_r^2},$$

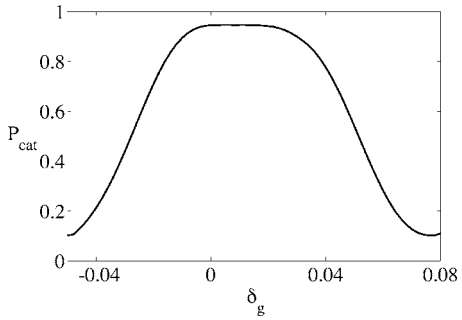


FIG. 6. The measurement $P_{cat}$ versus interaction strength variation, with $g=\tau/0.9N(1+\delta_g)$. Other system parameters and the projection operator is identical to Fig. 4. It is shown that in the vicinity of $\delta_g=0$, the cat state is created. Note that the projection is measured at different times for each $\delta_g$, so that the value of $P_{cat}$ is maximized.

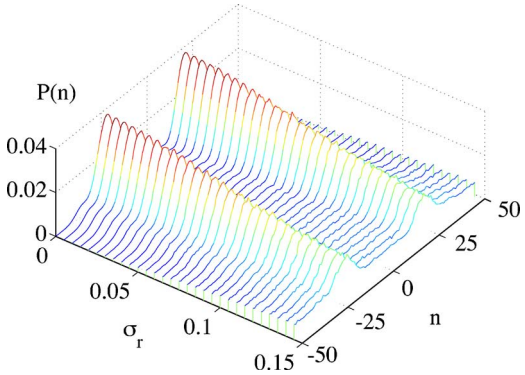


FIG. 7. (Color online) The probability distribution $P(n)$ at time $t=t_{cat}$ is plotted versus the level of random noise in the initial state $\sigma_r$. We see that even at $\sigma_r=0.05$ the output state is still a good cat state. This corresponds to random fluctuations in the initial $c_n$'s at about 5% of their exact ground-state values.

$$P(\theta) = \frac{1}{2\pi}. \tag{18}$$

Figure 7 shows the resulting cat state as a function of $\sigma_r$. We see that a well peaked cat state can be produced up to $\sigma_r \approx 0.05$, which is about $c_0(t=0)/6$, i.e, about one sixth of the peak value of the initial wave packet where we make the cat state from. Thus this method of generating a cat state appears robust against noise in the initial state, which could be due to a finite temperature (see Fig. 8).

Another possible source of error in creating the cat state is from the inaccuracy in control of the atomic interaction strength $g$ and/or the tunneling rate $\tau$. This effect is simulated by adding a Gaussian-distributed random number to negative $g$. We note that this is not equivalent to time-dependent fluctuations in $g$ and $\tau$, but rather represents imprecision in the control over the values of the parameters. The result is shown in Fig. 9, where it is seen that the evolution system is sensitive to the noise of the atomic interaction $g$, with only about ±2% deviation being tolerable. However, it does not necessarily mean that one cannot create a cat state without the well defined $g$. Instead, when $g$ is shifted, the time needed to create cat state $t_{cat}$ is also shifted, and one can still

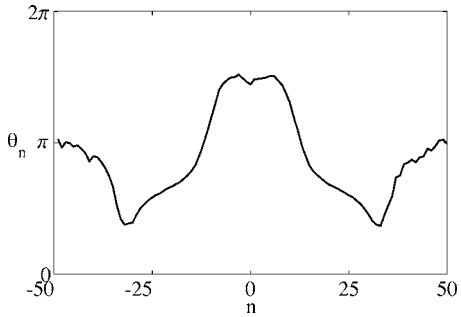


FIG. 8. The phase distribution $\theta_n=\arg(c_n)$ at $t=t_{cat}$ is plotted for the case of random noise in the initial state with $\sigma_r=0.05$. We see that the phase distribution agrees well with Fig. 5 up to a nonphysical overall phase shift. The disagreement occurs only in the regions where the amplitude of $c_n$ is small.

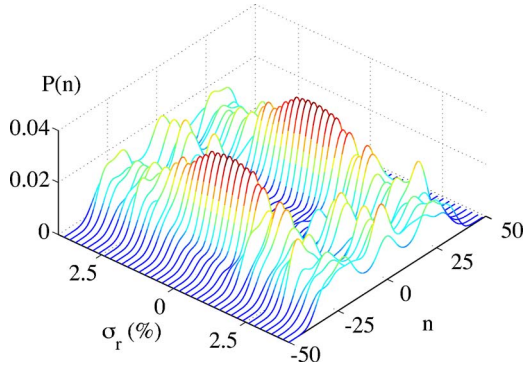


FIG. 9. (Color online) The effect of imprecise control over the atomic interaction strencth $g$. The noise of $g$ is introduced by adding a real random number, where $\sigma_r$ is the width of the corresponding Gaussian distribution, to the value of $g$ in Hamiltonian (4). The cat state is measured at a time of $t=14.5/\tau$ and plotted as a function of $\sigma_r$. It is shown that uncertanties in $g$ up to 3% can be tolerated.

obtain the cat state in another time. The primary difficulty here is that if the variation in $g$ is unknown for a given run, then the precise time to stop the dynamics, $t_{cat}$ is not known *a priori*.

## IV. DETECTION OF CAT STATE

Presuming a catlike state can be created in the above manner, it remains a challenge to experimentally verify the coherence between the macroscopically distinguishable states. Neverthless, a possible method to detect Schrödinger cat states in this bimodal BEC's lies in detecting the revival of the initial coherent state. In Fig. 10 we show the evolution of the cat state starting from $t=t_{cat}$ with the system parameters still satisfying $g=\tau/0.9N$. This shows that under the condition of no decoherence, the system will evolve back to a coherent state after a certain period of time, which we denote as $t_{rev}$. The revival time $t_{rev}$ again is estimated from our simulations, yielding $t_{rev}=7/\tau$.

In the presence of decoherence, however, the system may not be exhibit a distinct revival of the coherent state. To

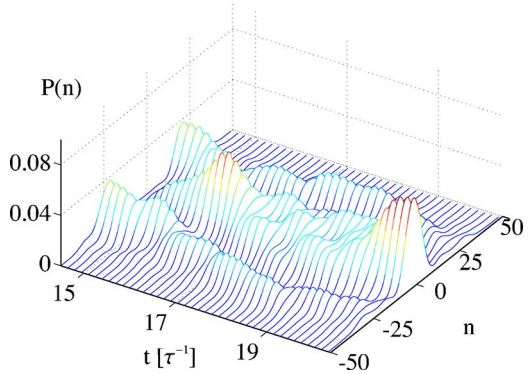


FIG. 10. (Color online) Revival dynamics from the cat state back to the coherent state. This figure shows the continued dynamical evolution following that shown in Fig. 3 with $g=-0.01$. At $t=14.5/\tau$, the quantum system is in a cat state, then at a time of $t \approx 21/\tau$, the initial coherent state is revived.

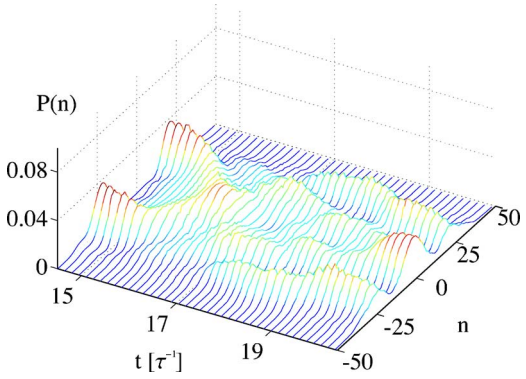


FIG. 11. (Color online) Dynamical evolution of a partially incoherent cat state. The parameters chosen are the same as Fig. 10. At $t=14.5/\tau$, the quantum system is in a mixed state with no coherence between the two wave packets. Then as it evolves, the system exhibits oscillations, but will not evolve back to the initial state.

illustrate this we first consider two states which we define as the partially incoherent state and the totally incoherent state. These states are defined by the introduction of a coherence "length" in Fock space, $I_{coh}$, so that coherent superpositions between Fock states $|n\rangle$ and $|m\rangle$ are destroyed for $|n-m| \gg I_{coh}$, while superpositions satisfying $|n-m| \lesssim I_{coh}$ are relatively unaffected by decoherence. The partially incoherent state is then defined in the sense that the coherence length $I_{coh}$ is small compared to the distance between the two separated peaks of the cat state, but larger than the width of either wave packet, i.e., $I_{coh} < n_0$ yet $I_{coh} > \sigma$ in Eq. (9). For the completely incoherent state, on the other hand, the cat state is taken to have collapsed to a single Fock state, i.e. a mixed state maintaining the probability distribution of the cat state but with to coherence between Fock states.

The evolution of those two states in time is shown in Figs. 11 and 12, respectively. Unlike the cat state, the incoherent states will not exhibit a revival of the initial coherent state at $t=t_{rev}$. The partially incoherent state evolves instead into a disinct three-peaked state, whereas the completely incoherent state exhibits small oscillations with no discernable peaks after a very short collapse time.

Based on these considerations, one prospective method to verify the coherence of the cat state would involve: (i) first, measuring the probability distribution, $P(n)$, which is accomplished by repeated measurements of the atom number in each mode; (ii) then after forming the cat state, the state should be held at $\tau=0$ for a time $t=t_{hold}$ and then with tunneling restored, the revival of the initial coherent state should be observed after a time $t_{rev}$; (iii) a known source of decoherence should be added while holding the system at $\tau=0$ for duration $t_{hold}$, after which a lack of revival should be observed. To add decoherence, one could simply add a laser field to the system. This will introduce decoherence due to spontaneous photon scattering, as described in Sec. V. If the revival of the initial state can be observed in the case of no additional decoherence, but disappears when the decoherence is added in a controlled way, than one should have a strong claim for the observation of coherence between macrscopically distinguishable states.

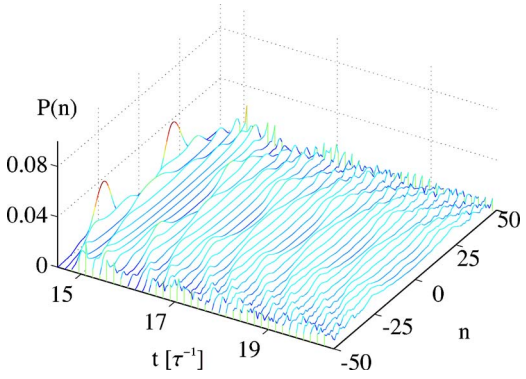


FIG. 12. (Color online) Dynamic evolution of the completely decoherent cat state. At $t=14.5/\tau$, we let the system collapse onto a statistical mixture of Fock states. It is seen that the dynamic is completely disordered.

## V. LASER-INDUCED DECOHERENCE AND LOSSES

While trapped ultracold atoms are typically well isolated from the environment, the presence of lasers for trapping and/or detection of atoms will polarize the atoms and thus couple them to the vacuum modes of the electromagnetic field. This coupling allows for spontaneous Rayleigh scattering and/or diffraction of laser photons, which can lead to losses and/or decoherence of the atomic system. If the scattered light field acquires sufficient information to determine the atom-number difference between the left and right wells, then this spontaneous scattering will lead to a dynamical collapse from the cat state into a mixture of Fock states, an example of environmentally induced decoherence.

In addition, the condensates are in contact with a thermal cloud on noncondensed atoms. In [42], it was determined that such a coupling will lead to a rapid collapse of the cat state. We note, however, that the treatment in [42] made the approximation that correlations between the condensate and the cloud decay much faster than the time scale of the condensate dynamics, i.e., the thermal cloud was treated as a Markovian reservoir. At present we question the validity of the Markov approximation for such a system. The coherence time can be quite long because (i) the cloud temperature is very low and the cloud is very dilute (so that collisions between cloud atoms are rare), and (ii) the cloud is confined, so that information does not propagate away from the condensate region. A non-Markovian treatment of thermal-cloud-induced decoherence is beyond the scope of this work. At present, we focus primarily on the decoherence induced by coupling to the electromagnetic field.

The structure of this section is as follows: in Sec. V A, we will first investigate the decoherence mechanics of condensates induced by laser scattering, where the general master equation is derived. Then, in Sec. V B, we discuss the condensate losses due to the inelastic collision, and the loss rate is obtained for one-mode condensate. In Sec. V C, we show the decoherence of the two-mode cat states in the elastic scattering regime, defined as the regime where the photon recoil is not sufficiently strong to remove the atom from its initial center-of-mass state. The system dynamics under this loss-less decoherence is studied in Sec. V D. Lastly, the

atom-loss and decoherence of cat states in the inelastic regime is studied in Sec. V E, where we find that the cat states created via dynamic evolution are less susceptible to decoherence-induced collapse than the extreme cat state, i.e., the true ground state of the system, which we have argued is inaccessible via adiabatic evolution.

### A. Master equation

If there is an optical component to the trapping potential, the atoms in the BEC will have an induced electric dipole moment which oscillates at the laser frequency. This dipole moment will couple the atoms to the electromagnetic vacuum, resulting in spontaneous Rayleigh scattering and/or diffraction of the laser beam. In addition, there will be laser-induced many-atom effects, primarily dipole-dipole interactions and collective effects such as superradiance. As we will see, these effects will lead to decoherence and collapse of the cat states, even in the absence of recoil-induced losses from the two cat modes. This decoherence is associated with the possibility for scattered and/or diffracted photons to carry away information sufficient to reveal the distribution of atoms between the two modes.

In order to model these effects we need to derive the master equation which governs the density operator of the atomic field. In the presence of laser coupling to a BEC system, the total Hamiltonian for the system, which includes the Hamiltonian for the atoms in condensate $H_s$, the reservoir of vacuum electromagnetic field $H_s$, and the interaction between them in the dipole approximation $V_{sr}$ can be written as

$$H = H_s + H_r + V_{sr}, \tag{19}$$

$$H_s = \int d^3r \Delta \hat{\Psi}_e^\dagger(\mathbf{r})\hat{\Psi}_e(\mathbf{r}) + \int d^3r\, \Omega(\mathbf{r})\hat{\Psi}_e^\dagger(\mathbf{r})\hat{\Psi}_g(\mathbf{r}), \tag{20}$$

$$H_r = \sum_{k\lambda} \omega_k \hat{a}_{\mathbf{k}\lambda}^\dagger \hat{a}_{\mathbf{k}\lambda}, \tag{21}$$

$$V_{sr} = \sum_{k\lambda} \int d^3r g_{k\lambda} e^{i\mathbf{k}\cdot\mathbf{r}} e^{i\omega_L t} \hat{\Psi}_e^\dagger(\mathbf{r})\hat{\Psi}_g(\mathbf{r})\hat{a}_{\mathbf{k}\lambda} + \text{H.c.}, \tag{22}$$

where $\hat{\Psi}_e(\mathbf{r})$ and $\hat{\Psi}_g(\mathbf{r})$ are the annihilation operators for atoms in the excited and ground states respectively, and $\hat{a}_{\mathbf{k}\lambda}$ is the photon annihilation operator for momentum $\hbar\mathbf{k}$ and polarization state $\lambda$. In addition, $\omega_e$, $\omega_L$, and $\omega_k$ denote the frequency of atomic excited state, laser field, and the reservoir photons, respectively, while $\Delta = \omega_e - \omega_L$ is the detunning of laser field from the excited state. The atom-laser interaction is governed by the Rabi frequency $\Omega(\mathbf{r})$, while the atom-reservoir interaction is governed by $g_{k\lambda} = \sqrt{(\omega_k/2\hbar\epsilon_0 V_e)}\mathbf{d}\cdot\boldsymbol{\epsilon}_{k\lambda}$, with $\mathbf{d}$ being the atomic dipole moment in mks units. We note that for the purpose of deriving the master equation it is not necessary to include terms in $H_s$ governing the free evolution of the ground state, as this involves very slow time scales relative to the dynamics of the excited-state and/or electromagnetic (EM)-vacuum system. These terms can be added to the system Hamiltonian at the end of the calculation, as any energy shifts they introduce will be negligible compared to the natural linewidth of the excited state.

The quantum state of the system plus reservoir is described by the density operator $\rho_{sr}$. An effective equation of motion for the reduced system density operator, $\rho_s = \text{tr}_r\{\rho_{sr}\}$, can be derived via second-order perturbation theory by following the standard approach (see, for example, [50]). For the case of a zero-temperature bath this leads directly to the master equation [51]

$$\dot{\rho}_s(t) = -iH_s\rho_s(t) - \int d^3r\, d^3r' \Big[ L(\mathbf{r} - \mathbf{r}')\hat{\Psi}_e^\dagger(\mathbf{r})\hat{\Psi}_g(\mathbf{r})\hat{\Psi}_g^\dagger(\mathbf{r}')\hat{\Psi}_e(\mathbf{r}')\rho_s(t) - L^*(\mathbf{r} - \mathbf{r}')\hat{\Psi}_g^\dagger(\mathbf{r})\hat{\Psi}_e(\mathbf{r})\rho_s(t)\hat{\Psi}_e^\dagger(\mathbf{r}')\hat{\Psi}_g(\mathbf{r}') \Big] + \text{H.c.}, \tag{23}$$

where

$$L(\mathbf{r} - \mathbf{r}') = \sum_{k\lambda} |g_{k\lambda}|^2 e^{i\mathbf{k}\cdot(\mathbf{r}-\mathbf{r}')} \left\{ \pi\delta(\omega_k - \omega_L) + \frac{i\mathcal{P}}{\omega_k - \omega_L} \right\}, \tag{24}$$

with $\mathcal{P}$ indicating a principal value. In the limit of infinite quantization volume, the summation becomes an integral, which can be done analytically [52], yielding

$$L(\mathbf{r} - \mathbf{r}') = \frac{3\Gamma}{4} e^{-i\zeta} \left( \sin^2\theta \frac{i}{\zeta} + (1 - 3\cos^2\theta)\left[ \frac{1}{\zeta^2} - \frac{i}{\zeta^2} \right] \right), \tag{25}$$

where $\Gamma = \omega_L^3 d^2/(3\pi\epsilon_0\hbar c^3)$ is the single-atom spontaneous emission rate, $\zeta = k_L|\mathbf{r} - \mathbf{r}'|$ and $\theta$ is the angle between the dipole moment $\mathbf{d}$ and $\mathbf{r} - \mathbf{r}'$. The real part of $L(\mathbf{r} - \mathbf{r}')$ will contribute to decoherence in the master equation (23), while the imaginary part contributes an energy shift due to photon exchange between atoms. In the limit $|\mathbf{r} - \mathbf{r}'| \to 0$ we find

$$L(0) = \frac{\Gamma}{2} + i\delta, \tag{26}$$

where the imaginary part $\delta$ is an infinite quantity, reflecting the fact that the standard two-level atom-field interaction model is not properly renomalized. Physically, this term is a Lamb-type shift in the energy of the excited state due to interaction with the vacuum modes of the EM field. In our system we can always choose a rotating frame to absorb this shift, so that we can take $\delta = 0$ without loss of generality.

For most optical traps, the laser is detuned very far from the atomic resonance frequency, so that the excited state occupation number is $\ll 1$. In this regime it is useful to perform an adiabatic elimination of the excited-state operators. The resulting master equation, involving only ground-state operators, is

$$\dot{\rho}_s(t) = -iH_s\rho_s(t) - i\int d^3r \frac{|\Omega(\mathbf{r})|^2}{\Delta}\hat{\Psi}^\dagger(\mathbf{r})\hat{\Psi}(\mathbf{r}) - \int d^3r\, d^3r' \Omega(\mathbf{r})\frac{L(\mathbf{r}-\mathbf{r}')}{\Delta^2}\Omega^*(\mathbf{r}')\hat{\Psi}^\dagger(\mathbf{r})\hat{\Psi}(\mathbf{r})\hat{\Psi}^\dagger(\mathbf{r}')\hat{\Psi}(\mathbf{r}')\rho_s(t)$$
$$+ \int d^3r\, d^3r' \Omega^*(\mathbf{r})\frac{L^*(\mathbf{r}-\mathbf{r}')}{\Delta^2}\Omega(\mathbf{r}')\hat{\Psi}^\dagger(\mathbf{r})\hat{\Psi}(\mathbf{r})\rho_s(t)\hat{\Psi}^\dagger(\mathbf{r}')\hat{\Psi}(\mathbf{r}') + \text{H.c.}, \tag{27}$$

where $\hat{\Psi}(\mathbf{r}) \equiv \hat{\Psi}_g(\mathbf{r})$. The details of this derivation are presented in the Appendix.

### B. Condensate losses: elastic and inelastic regimes

We will now employ this master equation to describe decoherence and/or atom loss in our two-mode atomic system. Underlying the dynamics governed by master equation (27) is the exchange of photons between atoms and between an atom and the EM vacuum. As such photon exchanges can involve significant momentum exchanges due to photon recoil, it is useful to first define elastic and inelastic regimes with respect to the initial atomic center-of-mass state. If the spatial size of the initial atomic mode is small compared to the laser wavelength, then one would be in the elastic regime, as photon recoil would not be sufficient to carry the atom outside of the momentum distribution of the initial state. In the inelastic regime, on the other hand, the initial mode is large compared to the laser wavelength, which implies that it is narrow in momentum space compared to the photon momentum, so that the recoil from a single photon is sufficient to remove an atom from its initial mode and place it in an orthogonal mode.

In the strongly elastic regime, there will be negligible loss of atoms from their initial modes. As we shall demonstrate, the master equation (27) may still lead to decoherence and/or collapse of the two mode cat states. In the inelastic regime, on the other hand, the predominant effect of the atom-field interaction will be scattering of atoms out of the initial modes and into a quasicontinuum of modes. This loss will be accompanied by a collapse of state of the remaining atoms into a mixture of states, which may or may not be catlike in themselves. The details of this decoherence process are given in Sec. V E.

To derive the atom decay rate of a single atomic-field mode, we will need to make use of the commutation relation

$$[\hat{c}^\dagger\hat{c}, \hat{\Psi}^\dagger(\mathbf{r})\hat{\Psi}(\mathbf{r})] = -\phi(\mathbf{r})\hat{c}^\dagger\hat{\Psi}(\mathbf{r}) - \phi^*(\mathbf{r})\hat{\Psi}^\dagger(\mathbf{r})\hat{c}, \tag{28}$$

where $\hat{c}$ is the annihilation operator for atoms in mode $\phi(\mathbf{r})$. Then, from the master equation (27), it is straight forward to obtain the evolution of the mean mode occupation $n_0 = \langle\hat{c}^\dagger\hat{c}\rangle$ as

$$\dot{n}_0 = -\int d^3r\, d^3r' \frac{G(\mathbf{r},\mathbf{r}')}{\Delta^2}[\phi^*(\mathbf{r})\delta^3(\mathbf{r}-\mathbf{r}')\langle\hat{c}^\dagger\hat{\Psi}(\mathbf{r}')\rangle$$
$$- \phi(\mathbf{r})\phi^*(\mathbf{r}')\langle\hat{\Psi}^\dagger(\mathbf{r})\hat{\Psi}(\mathbf{r}')\rangle + \phi^*(\mathbf{r})$$
$$\times\langle\hat{c}^\dagger\hat{\Psi}^\dagger(\mathbf{r}')\hat{\Psi}(\mathbf{r})\hat{\Psi}(\mathbf{r}')\rangle - \phi(\mathbf{r})\langle\hat{\Psi}^\dagger(\mathbf{r})\hat{\Psi}^\dagger(\mathbf{r}')\hat{\Psi}(\mathbf{r}')\hat{c}\rangle], \tag{29}$$

where $G(\mathbf{r},\mathbf{r}') = \Omega(\mathbf{r})L(\mathbf{r}-\mathbf{r}')\Omega^*(\mathbf{r}')$. Making a single mode approximation,

$$\hat{\Psi}(\mathbf{r}) = \phi(\mathbf{r})\hat{c}, \tag{30}$$

one obtains

$$\dot{n}_0 = -\frac{2}{\Delta^2}\int d^3r\, d^3r'\ \mathrm{Re}[G(\mathbf{r},\mathbf{r}')]|\phi(\mathbf{r})|^2$$
$$\times[\delta^3(\mathbf{r}-\mathbf{r}') - |\phi(\mathbf{r}')|^2]n_0. \tag{31}$$

To better understand the physics described by this equation, we make the simplifying assumption $\Omega(\mathbf{r}) \approx \Omega e^{i\mathbf{k}_L\cdot(\mathbf{r}-\mathbf{r}')}$, where $\mathbf{k}_L$ is the laser wave vector, satisfying $\mathbf{k}_L\cdot\mathbf{d}=0$. This leads to

$$\dot{n}_0 = -\frac{|\Omega|^2}{\Delta^2}\Gamma(1-\xi)n_0, \tag{32}$$

where

$$\xi = \frac{2}{\Gamma}\int d^3\, r d^3r'\ \mathrm{Re}[e^{i\mathbf{k}_L\cdot(\mathbf{r}-\mathbf{r}')}L(\mathbf{r}-\mathbf{r}')]|\phi_g(\mathbf{r})|^2|\phi_g(\mathbf{r}')|^2. \tag{33}$$

In the elastic regime we have $|\phi(\mathbf{r})|^2 \approx \delta(\mathbf{r})$ relative to $L(\mathbf{r}-\mathbf{r}')$, which leads to $\xi=1$ so that there is no atomic loss, as expected. As the size of the condensate grows, $\xi$ will decrease, as shown in Fig. 13, which plots $\xi$ versus the condensate size for the case of a spherically symmetric Gaussian condensate wave fuction

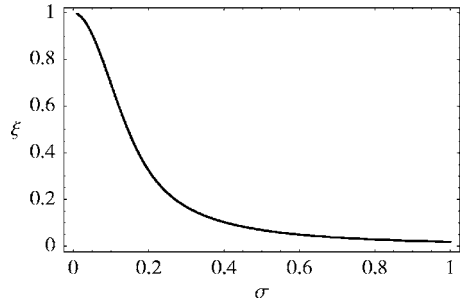


FIG. 13. Dependence of the inelastic loss parameter $\xi$ on the spatial size of the condensate, which is indicated by the dimensionless parameter $\sigma$ as shown in Eq. (34). It is seen that $\xi$ is approximately unity when the size of the condensate is much less than the laser wavelength, i.e., $\sigma \ll 1$, which means there is negligible atom loss. As the condensate size approaches half $\lambda_L$, $\xi$ decreases to around 0, corresponding to the maximum loss rate.

$$\phi(\mathbf{r}) = \frac{1}{(\sigma\lambda_L)^{3/2}\pi^{3/4}} e^{-r^2/(2\sigma^2\lambda_L^2)}, \tag{34}$$

where $\sigma$ is the ratio of the condensate size to the laser wavelength, $\lambda_L$. From the figure, we see that the decay rate of the condensate can be neglected under the condition $\sigma \ll 1$, while for a mode whose size is comparable to or larger than the laser wavelength, we have $\xi \to 0$ so that the population will decay at the expected rate $|\Omega|^2\Gamma/\Delta^2$, which is simply the electronically excited state fraction times the excited state lifetime.

### C. Decoherence of two-mode cat states in elastic regime

In the present scheme, $N$ atoms are trapped in a double-well potential with a finite spatial separation between the wells. Coupling of this system to the EM vacuum modes will result in decoherence only when scattered photons carry away sufficient information about the number of atoms in each well. It thus follows that if the separation between the two condensates, $s$, is less than the laser wavelength $\lambda_L$, no decoherence should occur, as the information contained in the photons is diffraction-limited to a resolution of no better than a wavelength. On the other hand, if $s$ is larger than $\lambda_L$, the locations of the atoms can, in principle, be determined from the phase information contained in the scattered photons, this irreversible transfer of information to the environment will be reflected in decoherence of Fock-space superpositions of different atom-number distributions.

In the deeply elastic regime, the size of the left and right modes is the smallest length scale in the problem, so that we can replace the atomic density distributions with $\delta$-functions, or equivalently we take

$$\hat{\Psi}(\mathbf{r}) = \sqrt{\delta\left(\mathbf{r} - \frac{\mathbf{s}}{2}\right)}\hat{c}_L + \sqrt{\delta\left(\mathbf{r} + \frac{\mathbf{s}}{2}\right)}\hat{c}_R, \tag{35}$$

where $\hat{c}_L$ and $\hat{c}_R$ are the annihilation operators for the left and right mode, respectively. Inserting this expansion into the master equation (27) and assuming again for simplicity $\Omega(\mathbf{r}) = \Omega e^{i\mathbf{k}_L\cdot\mathbf{r}}$, gives

$$\begin{aligned}\dot{\rho}_s = -\frac{|\Omega|^2\Gamma}{2\Delta^2}[&\hat{c}_L^\dagger\hat{c}_L\hat{c}_L^\dagger\hat{c}_L\rho_s + \hat{c}_R^\dagger\hat{c}_R\hat{c}_R^\dagger\hat{c}_R\rho_s \\ &+ 2\cos(\mathbf{k}_L\cdot\mathbf{s})\mu(\mathbf{s})\hat{c}_L^\dagger\hat{c}_L\hat{c}_R^\dagger\hat{c}_R\rho_s - \hat{c}_L^\dagger\hat{c}_L\rho_s\hat{c}_L^\dagger\hat{c}_L - \hat{c}_R^\dagger\hat{c}_R\rho_s\hat{c}_R^\dagger\hat{c}_R \\ &- \cos(\mathbf{k}_L\cdot\mathbf{s})\mu(\mathbf{s})\hat{c}_L^\dagger\hat{c}_L\rho_s\hat{c}_R^\dagger\hat{c}_R \\ &- \cos(\mathbf{k}_L\cdot\mathbf{s})\mu(\mathbf{s})\hat{c}_R^\dagger\hat{c}_R\rho_s\hat{c}_L^\dagger\ \hat{c}_L)] + \text{H.c.},\end{aligned} \tag{36}$$

where again the imaginary parts are absorbed via a transformation to the appropriate rotating frame. The resulting decoherence is governed by the parameter $\mu(\mathbf{s})$, defined as

$$\begin{aligned}\mu(\mathbf{s}) &\equiv 2\,\mathrm{Re}[L(\mathbf{s})]/\Gamma \\ &= \frac{3}{2}\left[\sin^2\theta_\mathbf{s}\frac{\sin\zeta}{\zeta} + (1 - 3\cos^2\theta_\mathbf{s})\left(\frac{\cos\zeta}{\zeta^2} - \frac{\sin\zeta}{\zeta^3}\right)\right],\end{aligned} \tag{37}$$

where $\zeta = 2\pi s/\lambda_L$ and $\theta_\mathbf{s}$ is the angle between the induced polarization direction $\mathbf{d}$ and the relative coordinate $\mathbf{s}$.

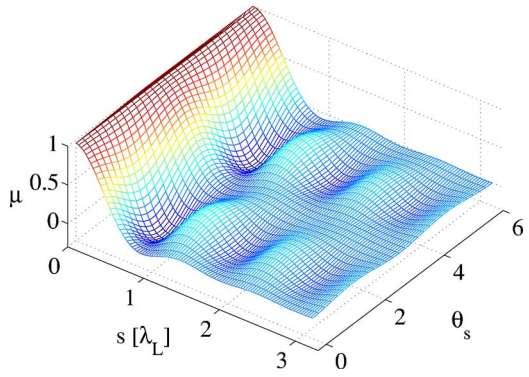


FIG. 14. (Color online) The decoherence parameter $\mu(\mathbf{s})$ as a function of $\theta_\mathbf{s}$ and $s/\lambda_L$. From the diagram, $\mu(\mathbf{s})$ is approximately 1 when the separation of two modes $s$ is much smaller than the laser wavelength $\lambda_L$. As $s$ increases, $\mu(\mathbf{s})$ decreases at a speed of $1/s$ and eventually approaches zero as $s$ goes much larger than $\lambda_L$. Note that $\mu(\mathbf{s})$ is also dependent on $\theta_\mathbf{s}$, where at large $s$, $\mu(\mathbf{s}) \sim \sin^2\theta_\mathbf{s}$.

From this master equation (36), we derive the equation of motion for the Fock-space matrix elements $\rho_{nm} = \langle n|\rho_s|m\rangle$, yielding

$$\dot{\rho}_{nm} = -\Gamma\frac{|\Omega|^2}{\Delta^2}(n-m)^2[1 - \cos(\mathbf{k}_L\cdot\mathbf{s})\mu(\mathbf{s})]\rho_{nm}. \tag{38}$$

This shows that the diagonal matrix elements $(m=n)$ do not decay, reflecting the absence of condensate losses in the elastic regime. The off-diagonal elements, on the other hand, decay as at a rate proportional to $[1-\cos(\mathbf{k}_L\cdot\mathbf{s})\mu(\mathbf{s})](n-m)^2$.

The dependence of $\mu(\mathbf{s})$ on the mode separation is shown in Fig. 14, which plots $\mu(\mathbf{s})$ versus $s/\lambda_L$ and $\theta_\mathbf{s} = \arg\mathbf{s}$. We see that under the condition of $s \ll \lambda_L$ we have $\cos(\mathbf{k}\cdot\mathbf{s})\mu(\mathbf{s}) \approx 1$, and therefore no decoherence. As $s$ increases, $\mu(\mathbf{s})$ will decrease and the decoherence rate will increase. In the limit of $s \gg \lambda_L$, we have $\mu(\mathbf{s}) \approx 0$, and the decoherence converges to the rate $\gamma_{nm} = |\Omega|^2/\Delta^2\Gamma(n-m)^2$. It is interesting to note that $\mu(\mathbf{s})$ is angle dependent, as seen in Fig. 14.

To understand the reason for this decoherence rate (38) we will consider the limiting cases $s \gg \lambda_L$ and $s \ll \lambda_L$, corresponding to a mode separation much larger than or much smaller than the laser wavelength, respectively. For the case where the mode separation is large compared to the laser wavelength, we have $\mu(\mathbf{s}) \to 0$ so that the decoherence rate is $\gamma_{nm} = (|\Omega|^2/\Delta^2)\Gamma(n-m)^2$. Our goal is thus to explain the peculiar $(n-m)^2$ dependence in this expression. We begin by noting that in this regime the phase information in the scattered photon wave fronts can, in principle, determine whether the photon scattered from the $L$ or the $R$ mode. Thus the question becomes: on what time scale $T$ does the radiation field scattered by $L$ or $R$ acquire sufficient information to distinguish the state $|n\rangle$ from the state $|m\rangle$. This time scale will then determine the decay rate for the off-diagonal elements $\rho_{nm}$, which give the degree of coherence between the states $|n\rangle$ and $|m\rangle$. The rate at which photons will scatter from

the left mode is $|\Omega|^2/\Delta^2\Gamma n_L^2$, where $n_L$ is the number of atoms in the left mode. The reason for the $n_L^2$ dependence, rather than the usual $n_L$, is due to the Bose stimulation, as the atoms remain in their initial mode after elastic scattering.

The actual scattering of photons is a random process, so that the number of $L$ scattered photons $n_p$ over a time interval $t$ is drawn from a distribution function $P_L(n_p,n_L,t)$. It is reasonable to assume that $P_L(n_p,n_L,t)$ is at least approximately Poissonian, with a center at $\bar{n}_p(n_L,t)=(|\Omega|^2/\Delta^2)\Gamma n_L^2 t$, and a width $\Delta n_p(n_L,t)=\sqrt{\bar{n}_p(n_L,t)}=(|\Omega|/\Delta)\sqrt{\Gamma t n_L}$. Based on this assumption, the criterion for distinguishing state $|n\rangle$ from state $|m\rangle$ is that the distributions $p_L(n_p,n_L,t)$ and $p_L(n_p,m_L,t)$ should be distinguishable, so that the scattered photon number can be attributed to one distribution or the other. In this expression $n_L$ is the number of atoms in mode $L$ for state $|n\rangle$ and This requires minimal overlap between the two distributions, which can be approximately formulated as

$$\bar{n}_p(n_L,T)+\Delta n_p(n_L,T)=\bar{n}_p(m_L,T)-\Delta n_p(m_L,T), \quad (39)$$

where we have temporarily assumed $m_L>n_L$. Solving this equation for the decoherence rate $\gamma_{nm}=1/t_d$ yields

$$\gamma_{nm}=\frac{|\Omega|^2}{\Delta^2}\Gamma\frac{[m_L^2-n_L^2]^2}{[m_L+n_L]^2}. \quad (40)$$

From Eq. (7) it follows that

$$n_L=\frac{N}{2}-n$$

$$n_R=\frac{N}{2}+n, \quad (41)$$

which also hold for $m_L$ and $m_R$ with a simple substitution $n\rightarrow m$. Inserting this into (40) yields

$$\gamma_{nm}=\frac{|\Omega|^2}{\Delta^2}\Gamma(n-m)^2. \quad (42)$$

We note that the result for mode $R$ instead of $L$ can be found via $n\leftrightarrow -n$ and $m\leftrightarrow -m$, while the result for $m_L<n_L$ can be found via $n\leftrightarrow m$, all of which leave the result (42) unchanged. Thus we have verified our interpretation that the decay of the $\rho_n m$ coherence is governed by the time scale on which the information carried by the scattered light becomes sufficient to distinguish between the states $|n\rangle$ and $|m\rangle$.

If we consider the opposite case $s\ll\lambda_L$ we can no longer assume that scattered photons carry information concerning which mode they scattered from, due to the standard diffraction limit. In this case one might be tempted to assume that the total scattering rate is proportional to $n_L^2+n_R^2=N^2/2+2n^2$, as photons must still scatter from one mode or the other and each mode will experience Bose stimulation of the recoiling atom. This would imply that the total scattering rate would be different for the states $|n\rangle$ and $|m\rangle$, so that given sufficient time the environment could learn which state is scattering the light and thus destroy the coherence. This effect, however, is compensated for by superradiance [53] so that the scattering rate is proportional simply to $N^2$, which is the same for both $|n\rangle$ and $|m\rangle$. Superradiance is a many-body quantum-interference effect whereby atoms within a distance less than the optical wavelength experience enhanced decay, identical to Bose stimulation, even for distinguishable atoms.

To verify this interpretation one can calculate the scattered light intensity and see precisely how it scales with $n_L$ and $n_R$. This can be accomplished by using Eqs. (21) and (22) to obtain the Heisenberg equation of motion for $\hat{a}_{\mathbf{k}\lambda}$,

$$\frac{d}{dt}\hat{a}_{\mathbf{k}\lambda}=-i\omega_k\hat{a}_{\mathbf{k}\lambda}-i\frac{\Omega}{\Delta}g_{\mathbf{k}\lambda}^*e^{-i\omega_L t}\int d^3r\, e^{i(\mathbf{k}_L-\mathbf{k})\cdot\mathbf{r}}\hat{\Psi}^\dagger(\mathbf{r})\hat{\Psi}(\mathbf{r}), \quad (43)$$

where we have substituted the adiabatic solution $\hat{\psi}_e(\mathbf{r})=(\Omega/\Delta)\hat{\Psi}(\mathbf{r})$. Substituting the mode expansion (35) and noting that $\hat{n}_L$ and $\hat{n}_R$ are constants of motion in the absence of tunneling gives upon time integration

$$\hat{a}_{\mathbf{k}\lambda}(t)=\hat{a}_{\mathbf{k}\lambda}(0)e^{-i\omega_k t}-i\frac{\Omega}{\Delta}g_{\mathbf{k}\lambda}^*e^{-i(\omega_k+\omega_L)t/2}\times\frac{\sin[(\omega_k-\omega_L)t/2]}{(\omega_k-\omega_L)/2}[e^{i(\mathbf{k}-\mathbf{k}_L)\mathbf{s}/2}\hat{n}_L+e^{-i(\mathbf{k}-\mathbf{k}_L)\mathbf{s}/2}\hat{n}_R]. \quad (44)$$

From this expression we can compute the mean number of scattered photons via $n_p(t)=\Sigma_{\mathbf{k}\lambda}\langle\hat{a}_{\mathbf{k}\lambda}^\dagger\hat{a}_{\mathbf{k}\lambda}\rangle$, yielding

$$n_p(t)=\frac{|\Omega|^2}{\Delta^2}\Gamma[n_L^2+n_R^2+2\cos(\mathbf{k}_L\cdot\mathbf{s})\mu(\mathbf{s})n_Ln_R]t, \quad (45)$$

where we have converted the sum to an integral in the limit of infinite quantization volume and made the approximation $\sin^2(xt)/x^2\approx\pi t\delta(x)$ when integrating over $k$. This expression reveals an additional component to the scattering rate proportional to $\cos(\mathbf{k}_L\cdot\mathbf{s})\mu(\mathbf{s})n_Ln_R$. This term is only significant when $\mu(\mathbf{s})\sim 1$, which requires that the mode separation be comparable to or less than the optical wavelength. In addition it depends on the exact spacing and orientation of the modes with respect to the polarization of the lasers, via the implied dependence of $\mu(\mathbf{s})$ on $\mathbf{s}$. We interpret this additional scattering as superradiance, as it arises from the imaginary part of the two-body dipole-dipole interaction. We see that in the limit as $s/\lambda_L\rightarrow 0$ we have $\cos(\mathbf{k}_L\cdot\mathbf{s})\mu(\mathbf{s})\rightarrow 1$ so that the total scattering rate is proportional to $N^2$. As stated previously, this means that the radiation field never acquires sufficient information to distinguish the states $|n\rangle$ and $|m\rangle$, therefore no decoherence occurs.

### D. Dynamics under decoherence in elastic regime

In the previous section, we derived the master equation of the two-mode system in the presence of laser-induced atomic polarization. In this section we use numerical simulations to observe how the decoherence will affect the tunneling dynamics of our system and determine what level of decoherence can be tolerated during the dynamical generation of a cat state. In this section we will only focus on the decoherent dynamics in this elastic regime where the total atom number can be treated as a constant of motion. In addition, we will assume that the mode separation is much larger than the laser

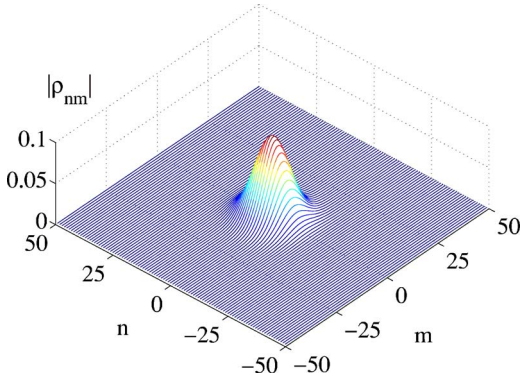


FIG. 15. (Color online) Magnitude of the density matrix elements for the initial coherent state.

wavelength, so that the dynamics is determined Eq. (38) but with $\mu_s=0$. Under those assumptions, it is straightforward to guess the coherence time $t_{coh}$ as

$$t_{coh}=\frac{4\Delta^2}{N^2|\Omega|^2\Gamma}, \tag{46}$$

by observing that the peaks of the dynamically created cat state are separated by $n_0=\pm N/4$. This is the time scale on which coherence between states separated by $N/4$ should decay based on the decoherence rate (42). During the generation of the cat state, it is expected that if the coherence time $t_{coh}$ is large compared to $t_{cat}$, the cat state can still be produced. Otherwise, the system should evolve into a mixed state rather than a pure cat state.

The effect of decoherence on the dynamical evolution of cat states is shown in Figs. 15–17. In Fig. 15 we show the magnitude of the density-matrix elements for the initial coherent state at $t=0$. Under the condition of no decoherence, this state evolves into a cat state at $t=t_{cat}$, which is shown in Fig. 16. In Figs. 17(a) and 17(b) we show the resulting state for the cases of weak and strong decoherence, respectively. In Fig. 17(a) the decoherence strength is chosen such that $t_{coh}=5t_{cat}$, while for the strong decoherence of Fig. 17(b), we have $t_{coh}=t_{cat}$. It is seen that with $t_{coh}=5t_{cat}$ we can still create catlike states, while as the decoherence strength increases

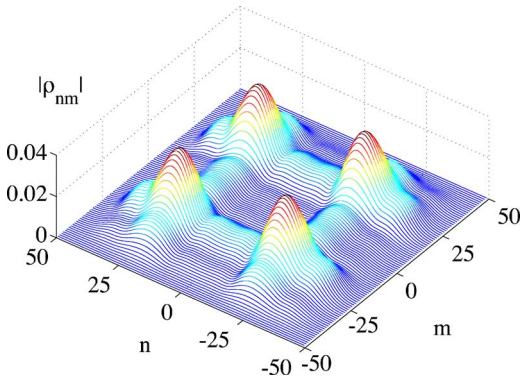


FIG. 16. (Color online) Magnitude of the density matrix elements of the dynamical created cat state at $t=t_{cat}$ with no decoherence.

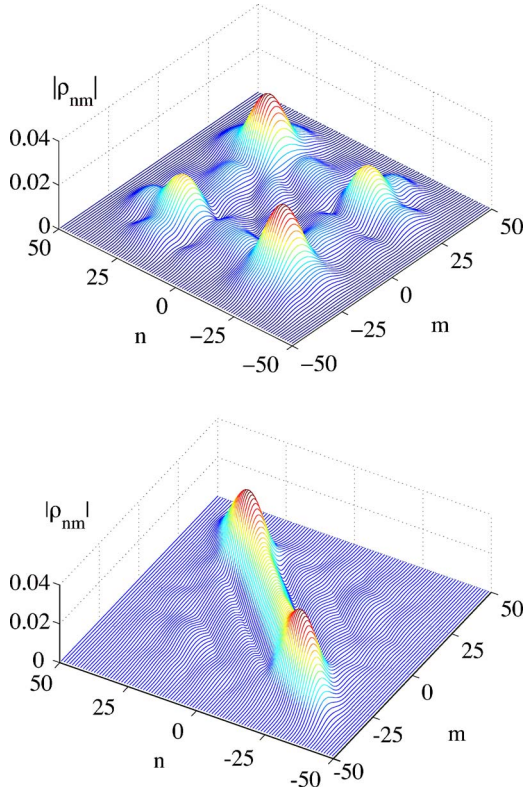


FIG. 17. (Color online) Magnitude of density-matrix elements of the resulting state under weak decoherence (a) and strong decoherence (b). System parameters are chosen the same as in Fig. 3, and the resulting states (a) and (b) are measured at a time of $t_{cat}=14.5/\tau$.

up to $t_{coh}=t_{cat}$, the outcome state is a mixted state with no coherence between macroscopically distinguishable distributiions. Therefore, to successfully produce a cat state, the coherence time $t_{coh}$ should be much longer than the time needed to produce cat state $t_{cat}$.

It is also quite interesting to observe from Fig. 17 that not only the off diagonal, but also the diagonal of density matrix of the final states are affected by the decoherence effect. In Fig. 18, we plot the probability distribution $P(n)\equiv\rho_{nn}$ of

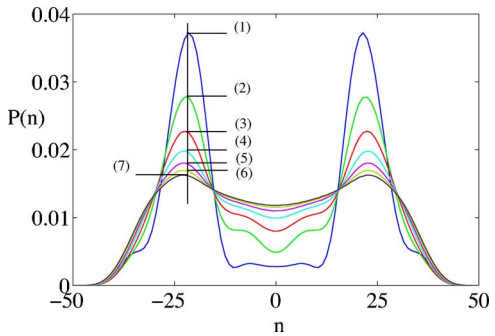


FIG. 18. (Color online) Probability distribution $P(n)$ of the resulting states corresponding to different coherence times. Parameters are chosen as in Fig. 17, while from line (1) to (7), the coherent time $t_{coh}$ is chosen as $\infty, 3t_{cat}, 3t_{cat}/2, t_{cat}, 3t_{cat}/4, 3t_{cat}/5, t_{cat}/2$, respectively.

several resulting states corresponding to different coherence times. In the figure we see that the probability distribution of the mixed states formed under strong decoherence is significantly different from that of the pure cat state. In other words, if decoherence dominates the system dynamics, it will not yield the same $P(n)$. This can be interpreted as a quantum-zeno effect, where tunneling is suppressed by decoherence, which effectively provides continuous measurement of the location of the atoms. Thus the probability distribution alone supplies a direct way to verify the existence of the cat state at time $t_{cat}$, without the need to detect revivals. We note that we have so far only established this result for the elastic regime. We suspect that the elastic regime will be much more difficult to achieve experimentally than the inelastic regime, due to the necessity of subwavelength confinement.

In Fig. 19 we examine the effects of decoherence on the revival process, under the assumption that $t_{cat} < t_{coh}$, but assuming that the system is held at $\tau=0$ for a time $t_{hold}$, which may be longer than the coherence time. These figures show the magnitude of the density-matrix elements at time $t=t_{cat}+t_{hold}+t_{rev}$, calculated by direct numerical solution of the master equation (36). In Fig. 19(a) we show the magnitude of the density-matrix elements for the case $t_{hold}=0$ and for $t_{coh}=\infty$, i.e., no decoherence is present. Note that this figure corresponds to $t=21$ in Fig. 10. In Fig. 19(b) we plot the magnitude of the resulting density matrix for the case $t_{hold}=t_{coh}=10t_{cat}$. This choice gives sufficient time to destroy coherence between Fock states where $n$ differs by $N/2$, corresponding to the distance between peaks in the initial cat state. This shows that the revival is effectively destroyed by decoherence on the time scale governed by the coherence time (46). This figure corresponds to the "partially incoherent state" shown in Fig. 11 at time $t=21$, in the sense that the choice $t_{hold}=t_{coh}$ implies the condition $\sigma < I_{coh} < n_0$. Lastly, Fig. 19(c) shows the case $t_{hold}=(N^2/4)t_{coh}$ with $t_{coh}=10t_{cat}$ which gives sufficient time to destroy coherence between any Fock states. We see in this case that the system has collapsed onto an almost pure mixture of Fock states, and it is clear that no revival occurs. This figure corresponds to the totally incoherent state of Fig. 12.

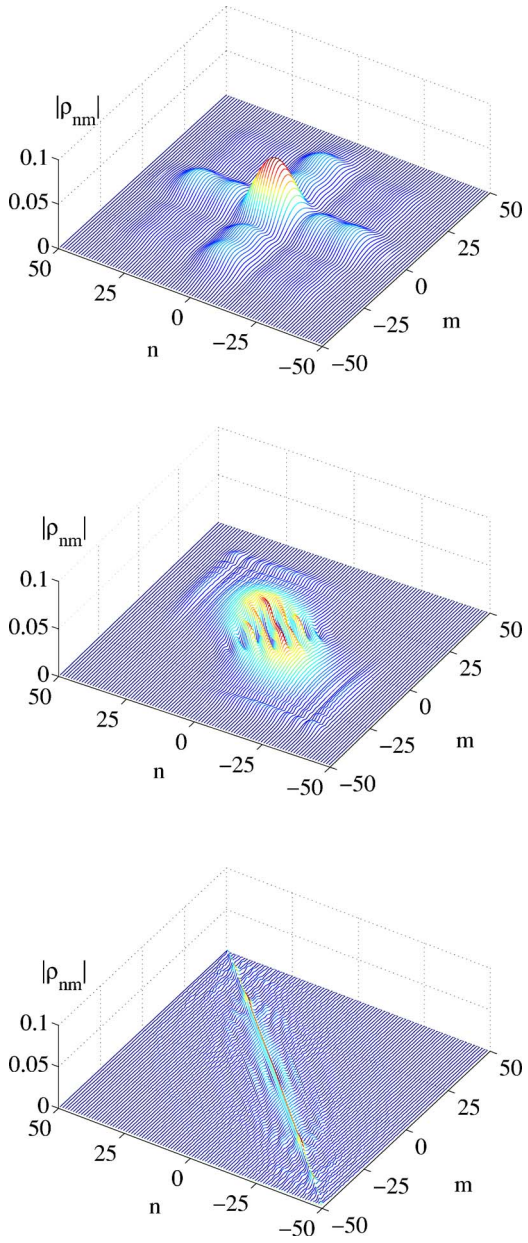


FIG. 19. (Color online) Effects of decoherence on the revival of the initial coherent state. Shown is the magnitude of the density-matrix elements of the system at time $t=t_{cat}+t_{hold}+t_{rev}$ under no decoherence (a), the decoherent resulting state with $t_{hold}=t_{coh}$ (b), and $t_{hold}=N^2t_{coh}/4$ (c). System parameters are chosen the same as in Fig. 3.

### E. Loss and decoherence in the inelastic regime

In this subsection we turn to the inelastic regime, which takes into account the finite size of the atomic modes, so that the scattering of laser photons is not entirely elastic due to photon recoil effects. The resulting losses from the two initially occupied modes should necessarily be accompanied by decoherence, which may or may not be sufficient to "collapse" the two-mode cat state. We focus solely on the case where the mode separation is large compared to the wavelength, so that we can safely ignore the cross terms in Eq. (36). The master equation in this situation is found by substituting the two-mode expansion $\hat{\Psi}(\mathbf{r})=\phi_L(\mathbf{r})\hat{c}_L+\phi_R(\mathbf{r})\hat{c}_R$, yielding

$$\dot{\rho}_s(t) = -\frac{|\Omega|^2\Gamma}{2\Delta^2}\{N\rho_s(t) + \xi[n_L^2 + n_R^2 - N]\rho_s(t) + \xi[n_L\rho_s(t)n_L + n_R\rho_s(t)n_R]\} + \text{H.c.}, \quad (47)$$

with $\xi$ defined in Eq. (33). Deriving the equation of motion for the density-matrix elements is then straightforward, giving

$$\dot{\rho}_{nm}(t) = -\Gamma\frac{|\Omega|^2}{\Delta^2}[(1-\xi)N + \xi(n-m)^2]\rho_{nm}(t). \quad (48)$$

Under the condition of spatially broad (relative to $\lambda_L$) condensates, $\xi \approx 0$, as seen if Fig. 13, and this equation is reduced to

$$\dot{\rho}_{nm}(t) = -\Gamma\frac{|\Omega|^2}{\Delta^2}N\rho_{nm}(t), \tag{49}$$

which shows that the decoherence rate is exactly equal to the atomic loss rate (32). The reason for this is that the loss of an atom takes us from the manifold with $N$ atoms to that with $N-1$ atoms. This is equivalent to $n \to n \pm 1$ where the choice of $\pm$ depends on whether the atom was lost from the $L$ or $R$ mode ($-$ for $L$ and $+$ for $R$). Thus one might suspect that a careful treatment of the scattering of the atom into the quasicontinuum of recoil modes would reveal that the loss of coherence on the matrix element $\rho_{nm}$ could be accompanied by a corresponding appearance of coherence on the matrix element $\rho_{n\pm1,m\pm1}$ which lies in the $N-1$ manifold.

A complete quantum description of this inelastic process should include both the initial cat state modes as well as a quasicontinuum of recoil modes. We can, therefore, describe the initial unscattered systems with a density of product $\rho_{sr}^N = \rho^N \otimes \rho_r$, where $\rho_{sr}^m$ is the full density operator having $m$ atoms in the initial modes and $N-m$ atoms in the quasicontinuum, and $\rho^m$ and $\rho_r^{N-m}$ are the corresponding reduced density matrices for the system and reservoir. After one photon is scattered, the full density matrix goes from $\rho_{sr}^N$ to $\rho_{sr}^{N-1}$, due to the transfer of one atom from the initial modes into the quasicontinuum. As the modes are well separated, the scattered photon carries sufficient phase information into the environment to determine whether the atom recoils from the $L$ or the $R$ mode. Assuming that atoms from $L$ and $R$ modes scatter into different manifolds of recoil modes, the reduced density operator of the two-mode system, obtained by tracing out the quasicontinuum modes, becomes

$$\rho^{N-1} = \frac{1}{\mathcal{N}}(c_L\rho^N c_L^\dagger + c_R\rho^N c_R^\dagger) \tag{50}$$

with $\mathcal{N}$ the normalization factor. In other words the system collapses onto an incoherence mixture of the state with one atom lost from mode $L$ and the state with one atom lost from mode $R$.

As an example, we now consider a $N$ particle cat state of

$$\rho^N = |\Psi_c\rangle\langle\Psi_c| \tag{51}$$

and to distinguish cat states with different total atom numbers, here we use a new notation

$$|\Psi_c\rangle = \frac{1}{\sqrt{2}}(|N/4,3N/4\rangle + |3N/4,N/4\rangle), \tag{52}$$

where $|n_L,n_R\rangle$ stands for a Fock basis with $n_L$ atoms in the left mode and $n_R$ in the right. This cat state is collapsed after one-photon detection into a statistical mixture of two $N-1$ particle states,

$$\rho^{N-1} = \tfrac{1}{2}(|\Psi_1\rangle\langle\Psi_1| + |\Psi_2\rangle\langle\Psi_2|) \tag{53}$$

where

$$|\Psi_1\rangle = \frac{1}{\sqrt{2}}(|N/4-1,3N/4\rangle + |3N/4-1,N/4\rangle), \tag{54}$$

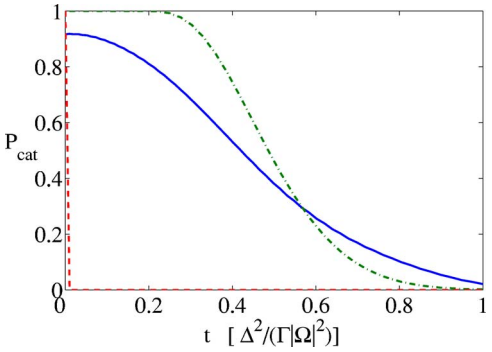


FIG. 20. (Color online) The evolution of the projector $P_{cat}$ under decoherence die to inelastic atom loss. The curves correspond to the dynamically created cat state (solid line), the perfect cat state (dashed line), and less extreme cat state (52) (dashed-dotted line). The figure plots the estimated probability to remain in a catlike state versus time. Starting from 100 atoms, it is estimated that 63 atoms are lost by the final time $t=\Delta^2/|\Omega|^2\Gamma$.

$$|\Psi_2\rangle = \frac{1}{\sqrt{2}}(|N/4,3N/4-1\rangle + |3N/4,N/4-1\rangle). \tag{55}$$

The important point here is that each of these states is still a good catlike state, so that while we do not know which one the system has collapsed into, we do know that the system remains in a good catlike state. The means that the effect of scattering a photon and losing an atom may not have a significant detrimental effect on catlike states. Similarly, after a second photon is scattered, the system will collapse into a statistical mixture of four $N-2$ particle cat states, and so on. We note, however, that for the "perfect" cat state $[|N0\rangle + |0N\rangle]/\sqrt{2}$ a single scattering results in a mixture of the states $|(N-1)0\rangle$ and $|0(N-1)\rangle$, neither of which is itself a cat state. This means that while the ideal cat state is so fragile that a single scattered photon is sufficient to collapse that cat onto all-left or all-right states, the catlike states we are considering should be significantly more robust, giving them a significant advantage provided they are still suitable for whatever application is desired.

To show the dynamics under decoherence induced by these inelastic condensate losses, in Fig. 20, we plot the time evolution of the expectation value of the projector $P_{cat}$, defined in (10). Three initial states are shown, the extreme cat state $[|N,0\rangle + |0N\rangle]/\sqrt{2}$, the less extreme cat state, $[|N/43N/4\rangle + |3N/4,N/4\rangle]/\sqrt{2}$ and the wave-packet cat states produced via dynamical evolution as in Sec. III B.

Figure 20 is obtained by assuming a single photon is detected in each time interval $\Delta t = \Delta^2/[|\Omega|^2\Gamma N(t)]$, where $N(t)$ is the number of remaining atoms at time $t$. After each scattering a new density matrix is obtained by applying Eq. (50). We note that the use of (50) automatically weighs the probabilities that the scattering occurs from the $L$ or $R$ mode due to the action of the annihilation operators being proportional to the square root of the mode occupation. The resulting density matrix is then diagonalized and written

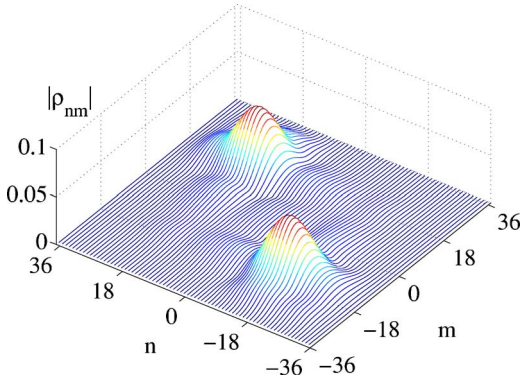


FIG. 21. (Color online) Magnitude of the resulting density-matrix elements corresponding to Fig. 20 at time $t=0.3\Delta^2/|\Omega|^2\Gamma$.

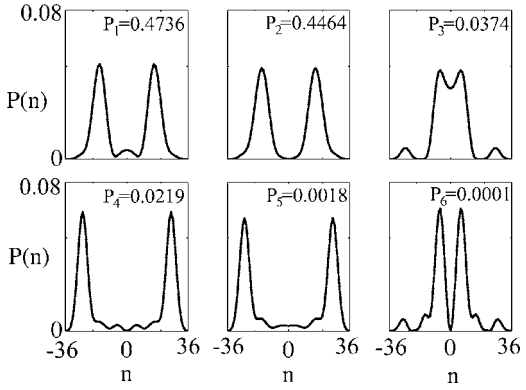


FIG. 22. Probability distributions $P(n)$ of the six leading eigenmodes of the density matrix shown in Fig. 21.

$$\rho = \sum_i P_i |\Psi_i\rangle\langle\Psi_i|, \tag{56}$$

where $|\Psi_i\rangle$ denotes the $i$th eigenmode, with $P_i$ its statistical weights over the mixture state. The resulting eigenmodes $|\Psi_i\rangle$'s are then analyzed to determine whether or not they are sufficiently catlike. This is accomplished by first assigning a value of zero to any state where $\Sigma_{n>0}|c_n|^2 \neq \Sigma_{n<0}|c_n|^2$, where $c_n$ is again the probability amplitudes for the state $|n\rangle$. The states which survive this test are then assigned a value equal to the expectation value of the projector $P_{cat}$. The assigned values for each eigenmode of the density matrix at time $t$ are then averaged together and the results are plotted versus time.

From the figure, we verify that the perfect cat state is completely collapsed immediately after one-photon scattering. In contrast, the less extreme cat states have a high probability to remain in a catlike state even after many scatterings, and, the dynamically created cat states are similarly robust against decoherence. We note that in the figure out of an initial population of $N=100$ atoms, $N=37$ remain at the end time $t=\Delta^2/|\Omega|^2\Gamma$.

In Fig. 21, we plot the magnitude of the density matrix after a time of $t_{hold}=0.3\Delta^2/|\Omega|^2\Gamma$ as in Fig. 20 (solid line). In this figure, an initial cat state is formed at time $t_{cat}$ via dynamic evolution with no decoherence. The state is then held with $g=0$ and $\tau=0$ for time $t_{hold}$ with photon-scattering acting as a gradual source of decoherence. The figure appears to show a collapse of the reduced density matrix onto a statistical mixture of left-centered and right-centered peaks. However, diagonalization of this matrix reveals that this is not the case. Based on numerical diagonalization, we plot the major eigenmodes $|\Psi_i\rangle$ of this density matrix in Fig. 22. From the picture, some of these resulting eigenmodes, such as $|\Psi_i\rangle$'s with $i=1,2,4,5$ are still catlike, in a sense that separation between two peaks are larger than the width of either peak. While for some others, like $|\Psi_3\rangle$ and $|\Psi_6\rangle$, the separation between peaks are not larger than the width of each peak, and thus they are not catlike. As more atoms are scattered, the number of remaining atoms decreases, and hence the maximum separation of catlike states will become will necessarily decrease. Because we have chosen projector $\hat{P}_{cat}$ to be fixed-width filter, those catlike states with small separations between peaks may not be picked by $\hat{P}_{cat}$. As a result, $P_{cat}$ decreases to almost zero before all atoms are lost, as seen in Fig. 20. Lastly, we note that in this section we did not show the effect of inelastic decoherence on the tunneling dynamics during the formation of the cat state. This can be done by the standard quantum jump method in Monto-Carlo simulation, which we plan to carry out in future work.

## VI. DEPHASING INDUCED BY ATOMIC COLLISIONS

In this section we consider the effects of atom-atom collisions on a cat state which is "frozen" by reducing the tunneling strength $\tau$ to zero. If during this hold time the atomic interaction strength $g$ is nonzero, the system will undergo a dephasing process [35,54,55], whose dynamics is determined by Hamiltonian (13). The main effect of this dephasing process is that, while it will not collapse the coherence of the cat state, once the state is dephased, it cannot evolve back to the initial coherent state. In this way, a detection scheme based on revivals will incorrectly create the appearance of collapse. Therefore, in general, the dephasing effect needs to be suppressed by making the atomic interaction strength $g$, and/or the hold time small.

In studying the dephasing effect, first, we note that at each period of $\pi/g$, the relative phase of each $c_n$ is exactly restored and thus the many-body states is revived. While between two consequent revivals, nonzero relative phases appear between Fock states, and the cat state will collapse. In Fig. 23, we show such a rapid dephasing process, where the cat state decays with a collapse time around $t_{col}=0.02/|g|$, determined from numerical simulations.

To obtain an analytic estimate of the collapse time scale, we assume that our system is prepared in a Gaussian-like cat state (9), which is a good approximation of the realistic cat state in our system. And then, we associate the collapse and revival of our bimodal system with the evolution of one-body two-mode correlation function $\Lambda$,

$$\Lambda = \langle \text{cat}|\hat{a}_L^\dagger \hat{a}_R|\text{cat}\rangle. \tag{57}$$

At a short time scale, the correlation function (57) is obtained, under the condition of that the Gaussians are well peaked around $n=\pm n_0$, to a good approximation [54],

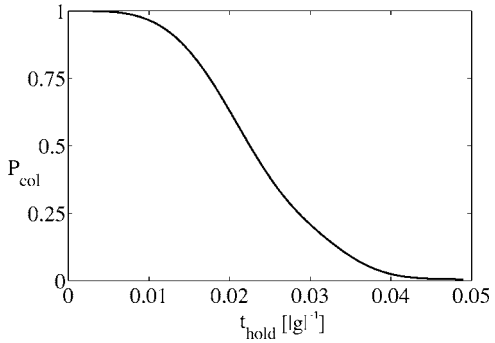


FIG. 23. Dephasing process of cat states with nonzero atomic interaction. The collapse is measured by $P_{col}=\mathrm{tr}\{\rho_c\rho(t)\}$, where $\rho_c$ and $\rho(t)$ are the densities of the initial cat state and dephased state after a hold time $t_{hold}$, respectively. Parameters are given the same as in Fig. 3, while $t_{hold}$ has units of $1/|g|$.

$$\Lambda(t) = \Lambda(0)e^{-(g\sigma t)^2} \tag{58}$$

and therefore, the collapse time $t_{col}$ can be estimated by

$$t_{col} = \frac{1}{2g\sigma}. \tag{59}$$

As discussed above, the collisional dephasing will affect the revival process. Generally speaking, if the holding time $t_{hold}$ is less than collapse time $t_{col}$, the system can still evolve back to the initial state as shown in Fig. 24(a). But under the condition of $t_{hold} > t_{col}$, the cat state is dephased, and the coherent state cannot be restored. Rather it will evolve to a disordered state as shown Fig. 24(b). Therefore, for the success of the detection scheme, one should make sure that the dephasing collapse time is longer than the hold time and the revival process is only affected by decoherence.

## VII. CONCLUSION

We have considered the double-well BEC system and proposed that catlike states can be formed by switching the sign of the interaction strength from positive to negative using a Feshbach resonance. We examined the possibility of either adiabatic or sudden switching with the following results. In the adiabatic case, the ground state evolves into a macroscopic superposition state with all of the atoms collectively occupying either the left or right well. However, by examining the degeneracy of the ground state, we conclude that the cat state is unstable against small perturbations and may readily evolve into a localized state. For the case of a sudden change in the scattering length, we find that an initial condensate state evolves dynamically into a double-peaked superposition of number states, with one peak corresponding to the majority of atoms being in one well, and the other peak corresponding to the majority being in the opposite well.

We have shown that this process is stable against perturbations in the initial state, as well as in the control parameters. For this reason we believe that the dynamical evolution scheme is more likely to be demonstrated experimentally. In addition, we have demonstrated that continuing the evolution after the cat state formation results in a nearly complete revival of the initial state. However, this revival does not occur if the cat state has collapsed into an incoherent mixed state, so that this revival can be taken as proof of coherence of the initial cat state. We note that the states formed via adiabatic switching are maximum "all or nothing" cat states, while those formed dynamically are less distinct catlike states corresponding to a double-peaked distribution in Fock space.

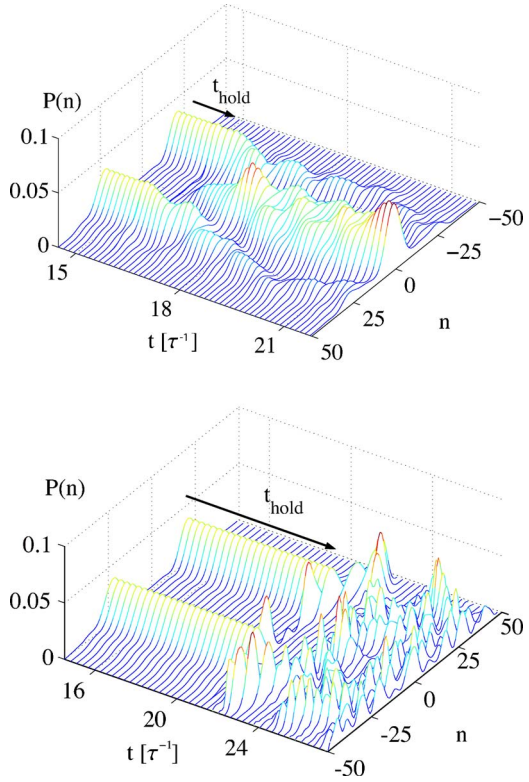


FIG. 24. (Color online) Dynamic evolution of dephased cat states after turning on the tunneling. The parameters are chosen as in Fig. 3 with a collapse time of $t_{col}=1.5/\tau$. In the first picture (a), the hold time is set to be $t_{hold}=t_{col}$, while for (b), we set $t_{hold}=5t_{col}$. It is shown that for (a), the system still revives to the initial state, while in (b), the initial state cannot be restored.

The effects of decoherence due to spontaneous scattering of laser photons have also been studied in detail. We have determined that decoherence is strongest for the case where the single-photon momentum recoil is not sufficient to remove the atom from its initial state, due to Bose stimulation as the atom remains in an strongly occupied atomic-field mode. In the opposite regime, where the scattering rate is smaller by a factor of $N$, $N$ being the atom number, we find that the maximally entangled all or nothing cat states are destroyed by the scattering of a single photon, while the dynamically formed less-extreme catlike states can survive multiple scatterings without leaving the subspace of catlike states, in analogy to the effect of atomic collision losses studied in [32]. Because of this enhanced survivability, the less-extreme cat states may be more useful for applications, providing they are suitable for the desired protocol.

In this context of freezing the cat states for a prolonged time, we have also considered the de-phasing effects of atom-atom interactions during this stage, and conclude that collisions can mimic the effects of decoherence with regard

to a revival-type measurement, however with regard to applications, they may or may not be detrimental, depending on the type of interaction and/or measurements involved.

We note that in the present proposal, there are three different time scales which we have established: the time need to create cat state $t_{cat}$, the coherence time $t_{coh}$, and the collisional dephasing time $t_{col}$. First, to generate the cat state, the coherence time scale $t_{coh}$ must longer than $t_{cat}$. While later, in order to hold the cat state for later use in an application, a hold time $t_{hold}$ shorter than $t_{coh}$ is required to maintain the macroscopic superposition state. And finally, another condition $t_{col} > t_{hold}$ should be satisfied to avoid the dephasing quasicollapse, if such dephasing is detrimental to the desired application. The coherence time $t_{coh}$ is tunable by adjusting the laser intensity and detuning, while the dephasing time $t_{dephase}$ can be adjusted if the interaction strength $g$ is modified during the hold stage.

## APPENDIX

To eliminate the excited state in the master equation (23), we note that for a far-off-resonant laser field, the excitation rate in BEC is extremely low, which enables us to expand the density matrix to a good approximation as

$$\rho \approx \rho_{00} + \rho_{01} + \rho_{10} + \rho_{11}, \tag{A1}$$

where $\rho_{00}$ and $\rho_{11}$ stand for the density matrix of no excitation and one excitation state, respectively, while $\rho_{01}$ and $\rho_{10}$ describe coherence between these two manifolds. In fact, it is convenient to define a projection operator $\hat{P}_j$, which is a projection into a subspace with $j$ atomic excitations of the BEC system, such that

$$\rho_{ij} = \hat{P}_i \rho \hat{P}_j. \tag{A2}$$

With this expansion, one obtains

$$\dot{\rho}_{00} = -i \int d^3r\, \Omega(\mathbf{r}) \hat{\Psi}_g^\dagger(\mathbf{r}) \hat{\Psi}_e(\mathbf{r}) \rho_{01} + \int d^3r\, d^3r'\, L(\mathbf{r}-\mathbf{r}') \times \hat{\Psi}_g^\dagger(\mathbf{r}) \hat{\Psi}_e(\mathbf{r}) \rho_{11} \hat{\Psi}_e^\dagger(\mathbf{r}') \hat{\Psi}_g(\mathbf{r}') + \text{H.c.}, \tag{A3}$$

$$\dot{\rho}_{10} = -i \int d^3r\, \Omega^*(\mathbf{r}) \hat{\Psi}_e^\dagger(\mathbf{r}) \hat{\Psi}_g(\mathbf{r}) \rho_{00} + i \int d^3r\, \Omega^*(\mathbf{r}) \rho_{11} \hat{\Psi}_e^\dagger(\mathbf{r}) \hat{\Psi}_g(\mathbf{r}) - \int d^3r\, d^3r'\, L(\mathbf{r}-\mathbf{r}') \hat{\Psi}_e^\dagger(\mathbf{r}) \hat{\Psi}_g(\mathbf{r}) \times \hat{\Psi}_g^\dagger(\mathbf{r}') \hat{\Psi}_e(\mathbf{r}') \rho_{10} - i\Delta\rho_{10}, \tag{A4}$$

$$\dot{\rho}_{01} = \dot{\rho}_{10}^\dagger, \tag{A5}$$

and

$$\dot{\rho}_{10} = -i \int d^3r\, \Omega^*(\mathbf{r}) \hat{\Psi}_e^\dagger(\mathbf{r}) \hat{\Psi}_g(\mathbf{r}) \rho_{01} - \int d^3r\, d^3r'\, L(\mathbf{r}-\mathbf{r}') \hat{\Psi}_e^\dagger(\mathbf{r}) \times \hat{\Psi}_g(\mathbf{r}) \hat{\Psi}_g^\dagger(\mathbf{r}') \hat{\Psi}_e(\mathbf{r}') \rho_{11} + \text{H.c.} \tag{A6}$$

In the assumption of low excitation rates, one can adiabatically eliminate $\rho_{01}$ and $\rho_{10}$ by demanding $\dot{\rho}_{01} \approx 0$ and $\dot{\rho}_{10} \approx 0$, respectively, yielding

$$\rho_{10} = -\int d^3r \frac{\Omega^*(\mathbf{r})}{\Delta} \hat{\Psi}_e^\dagger(\mathbf{r}) \hat{\Psi}_g(\mathbf{r}) \rho_{00} + \int d^3r \frac{\Omega^*(\mathbf{r})}{\Delta} \rho_{11} \hat{\Psi}_e^\dagger(\mathbf{r}) \hat{\Psi}_g(\mathbf{r}) i \int d^3r\, d^3r' \frac{L(\mathbf{r}-\mathbf{r}')}{\Delta} \times \hat{\Psi}_e^\dagger(\mathbf{r}) \hat{\Psi}_g(\mathbf{r}) \hat{\Psi}_g^\dagger(\mathbf{r}') \hat{\Psi}_e(\mathbf{r}') \rho_{10} \tag{A7}$$

Solving this equation perturbatively up to the order $1/\Delta^2$, one obtains

$$\rho_{10} = -\int d^3r \frac{\Omega^*(\mathbf{r})}{\Delta} \hat{\Psi}_e^\dagger(\mathbf{r}) \hat{\Psi}_g(\mathbf{r}) \rho_{00} + \int d^3r \frac{\Omega^*(\mathbf{r})}{\Delta} \rho_{11} \hat{\Psi}_e^\dagger(\mathbf{r}) \hat{\Psi}_g(\mathbf{r}) - i \int d^3r\, d^3r'\, d^3r'' \frac{L(\mathbf{r}-\mathbf{r}') \Omega^*(\mathbf{r}'')}{\Delta^2} \hat{\Psi}_e^\dagger(\mathbf{r}) \hat{\Psi}_g(\mathbf{r}) \hat{\Psi}_g^\dagger(\mathbf{r}') \hat{\Psi}_e(\mathbf{r}') \hat{\Psi}_e^\dagger(\mathbf{r}'') \hat{\Psi}_g(\mathbf{r}'') \rho_{00} + i \int d^3r\, d^3r'\, d^3r'' \frac{L(\mathbf{r}-\mathbf{r}') \Omega^*(\mathbf{r}'')}{\Delta^2} \hat{\Psi}_e^\dagger(\mathbf{r}) \hat{\Psi}_g(\mathbf{r}) \hat{\Psi}_g^\dagger(\mathbf{r}') \hat{\Psi}_e(\mathbf{r}') \rho_{11} \hat{\Psi}_e^\dagger(\mathbf{r}'') \hat{\Psi}_g(\mathbf{r}''), \tag{A8}$$

and $\rho_{01} = \rho_{01}^\dagger$. Inserting this result for $\rho_{01}, \rho_{10}$ back into Eq. (A6), we find

$$\dot{\rho}_{11} = i \int d^3r\, d^3r' \frac{\Omega^*(\mathbf{r}) \Omega(\mathbf{r}')}{\Delta} \hat{\Psi}_e^\dagger(\mathbf{r}) \hat{\Psi}_g(\mathbf{r}) \rho_{00} \hat{\Psi}_g^\dagger(\mathbf{r}') \hat{\Psi}_e(\mathbf{r}') - i \int d^3r\, d^3r' \frac{\Omega^*(\mathbf{r}) \Omega(\mathbf{r}')}{\Delta} \hat{\Psi}_e^\dagger(\mathbf{r}) \hat{\Psi}_g(\mathbf{r}) \hat{\Psi}_g^\dagger(\mathbf{r}') \hat{\Psi}_e(\mathbf{r}') \rho_{11} + \int d^3r\, d^3r'\, d^3r''\, d^3r''' \frac{L^*(\mathbf{r}''-\mathbf{r}') \Omega^*(\mathbf{r}) \Omega(\mathbf{r}''')}{\Delta^2} \hat{\Psi}_e^\dagger(\mathbf{r}) \hat{\Psi}_g(\mathbf{r}) \rho_{00} \hat{\Psi}_g^\dagger(\mathbf{r}''') \hat{\Psi}_e(\mathbf{r}''') \hat{\Psi}_e^\dagger(\mathbf{r}') \hat{\Psi}_g(\mathbf{r}') \hat{\Psi}_e^\dagger(\mathbf{r}'') \hat{\Psi}_e(\mathbf{r}'') - \int d^3r\, d^3r'\, d^3r''\, d^3r''' \frac{L^*(\mathbf{r}''-\mathbf{r}') \Omega^*(\mathbf{r}) \Omega(\mathbf{r}''')}{\Delta^2} \hat{\Psi}_e^\dagger(\mathbf{r}) \hat{\Psi}_g(\mathbf{r}) \hat{\Psi}_g^\dagger(\mathbf{r}''') \hat{\Psi}_e(\mathbf{r}''') \rho_{11} \hat{\Psi}_e^\dagger(\mathbf{r}') \hat{\Psi}_g(\mathbf{r}') \hat{\Psi}_g^\dagger(\mathbf{r}'') \hat{\Psi}_e(\mathbf{r}'')$$

$$+ i \int d^3r\, d^3r'\, L(\mathbf{r}-\mathbf{r}')\hat{\Psi}_e^\dagger(\mathbf{r})\hat{\Psi}_g(\mathbf{r})\hat{\Psi}_g^\dagger(\mathbf{r}')\hat{\Psi}_e(\mathbf{r}')\rho_{11} + \text{H.c.}. \tag{A9}$$

Nextt, we apply a similar adiabatic elimination process to eliminate the excited state matrix $\rho_{11}$. To do that, first we normal order the ground-state operators in above equation, and then by setting $\dot{\rho}_{11} \approx 0$, obtains

$$\begin{aligned}
\rho_{11} = {} & i \int d^3r\, d^3r' \frac{\Omega^*(\mathbf{r})\Omega(\mathbf{r}')}{2\Delta\Gamma}\hat{\Psi}_e^\dagger(\mathbf{r})\hat{\Psi}_g(\mathbf{r})\rho_{00}\hat{\Psi}_g^\dagger(\mathbf{r}')\hat{\Psi}_e(\mathbf{r}') - i \int d^3r\, d^3r' \frac{\Omega^*(\mathbf{r})\Omega(\mathbf{r}')}{2\Delta\Gamma}\hat{\Psi}_e^\dagger(\mathbf{r})\hat{\Psi}_g^\dagger(\mathbf{r}')\hat{\Psi}_g(\mathbf{r})\hat{\Psi}_e(\mathbf{r}')\rho_{11} \\
& - i \int d^3r \frac{|\Omega(\mathbf{r})|^2}{2\Delta\Gamma}\hat{\Psi}_e^\dagger(\mathbf{r})\hat{\Psi}_e(\mathbf{r})\rho_{11} - \int d^3r\, d^3r' \frac{L(\mathbf{r}-\mathbf{r}')}{2\Gamma}\hat{\Psi}_e^\dagger(\mathbf{r})\hat{\Psi}_g^\dagger(\mathbf{r}')\hat{\Psi}_g(\mathbf{r})\hat{\Psi}_e(\mathbf{r}')\rho_{11} \\
& + \int d^3r\, d^3r'\, d^3r'' \frac{L^*(\mathbf{r}''-\mathbf{r}')\Omega^*(\mathbf{r})\Omega(\mathbf{r}')}{2\Delta^2\Gamma}\hat{\Psi}_e^\dagger(\mathbf{r})\hat{\Psi}_g(\mathbf{r})\rho_{00}\hat{\Psi}_g^\dagger(\mathbf{r}')\hat{\Psi}_g(\mathbf{r}')\hat{\Psi}_g^\dagger(\mathbf{r}'')\hat{\Psi}_e(\mathbf{r}'') \\
& - \int d^3r\, d^3r'\, d^3r''\, d^3r''' \frac{L^*(\mathbf{r}''-\mathbf{r}')\Omega^*(\mathbf{r})\Omega(\mathbf{r}''')}{2\Delta^2\Gamma}\hat{\Psi}_e^\dagger(\mathbf{r})\hat{\Psi}_g(\mathbf{r})\hat{\Psi}_g^\dagger(\mathbf{r}''')\hat{\Psi}_e(\mathbf{r}''')\rho_{11}\hat{\Psi}_e^\dagger(\mathbf{r}')\hat{\Psi}_g(\mathbf{r}')\hat{\Psi}_g^\dagger(\mathbf{r}'')\hat{\Psi}_e(\mathbf{r}'') + \text{H.c.},
\end{aligned} \tag{A10}$$

Again, we solve this equation perturbatively up to order $1/\Delta^2$, and arrive at

$$\begin{aligned}
\rho_{11} = {} & \int d^3r\, d^3r'\, d^3r'' \frac{L^*(\mathbf{r}''-\mathbf{r}')\Omega^*(\mathbf{r})\Omega(\mathbf{r}')}{2\Delta^2\Gamma}\hat{\Psi}_e^\dagger(\mathbf{r})\hat{\Psi}_g(\mathbf{r})\rho_{00}\hat{\Psi}_g^\dagger(\mathbf{r}')\hat{\Psi}_g(\mathbf{r}')\hat{\Psi}_g^\dagger(\mathbf{r}'')\hat{\Psi}_e(\mathbf{r}'') \\
& - \int d^3r\, d^3r'\, d^3r''\, d^3r'''\, d^3r''''' \frac{L(\mathbf{r}-\mathbf{r}')L^*(\mathbf{r}'''''-\mathbf{r}''')\Omega^*(\mathbf{r}'')\Omega(\mathbf{r}''')}{2\Delta^2\Gamma^2}\hat{\Psi}_e^\dagger(\mathbf{r})\hat{\Psi}_g^\dagger(\mathbf{r}')\hat{\Psi}_g(\mathbf{r})\hat{\Psi}_e(\mathbf{r}')\hat{\Psi}_e^\dagger(\mathbf{r}'')\hat{\Psi}_g^\dagger(\mathbf{r}'')\rho_{00} \\
& \times \hat{\Psi}_g^\dagger(\mathbf{r}''')\hat{\Psi}_g(\mathbf{r}''')\hat{\Psi}_g^\dagger(\mathbf{r}''''')\hat{\Psi}_e(\mathbf{r}''''') - \int d^3r\, d^3r'\, d^3r''\, d^3r'''\, d^3r''''' \frac{L(\mathbf{r}-\mathbf{r}')L^*(\mathbf{r}'''''-\mathbf{r}''')\Omega^*(\mathbf{r}''')\Omega(\mathbf{r}'')}{2\Delta^2\Gamma^2} \\
& \times \hat{\Psi}_e^\dagger(\mathbf{r})\hat{\Psi}_g^\dagger(\mathbf{r}')\hat{\Psi}_g(\mathbf{r})\hat{\Psi}_e(\mathbf{r}')\hat{\Psi}_e^\dagger(\mathbf{r}''''')\hat{\Psi}_g^\dagger(\mathbf{r}''''')\hat{\Psi}_g^\dagger(\mathbf{r}''')\hat{\Psi}_g(\mathbf{r}''')\rho_{00}\hat{\Psi}_g^\dagger(\mathbf{r}'')\hat{\Psi}_e(\mathbf{r}'') + \text{H.c.}
\end{aligned} \tag{A11}$$

This expression for $\rho_{11}$ can be simplified by normal ordering. Finally, we insert the normal ordered $\rho_{01}, \rho_{01}, \rho_{11}$ back into Eq. (A3), and keep only terms up to $1/\Delta^2$. In addition, since the atomic density in BEC is low, we drop any three-body and above terms. With these two assumptions, we obtain the resulting master equation (27),

$$\begin{aligned}
\dot{\rho}_s(t) = {} & -iH_s\rho_s(t) - \frac{|\Omega|^2}{\Delta^2}\Gamma \int d^3r\, \hat{\Psi}_g^\dagger(\mathbf{r})\hat{\Psi}_g(\mathbf{r})\rho_s(t) - \int d^3r\, d^3r' \frac{\Omega(\mathbf{r})L(\mathbf{r}-\mathbf{r}')\Omega^*(\mathbf{r}')}{\Delta^2}\hat{\Psi}_g^\dagger(\mathbf{r})\hat{\Psi}_g^\dagger(\mathbf{r})\hat{\Psi}_g(\mathbf{r}')\hat{\Psi}_g(\mathbf{r}')\rho_s(t) \\
& + \int d^3r\, d^3r' \frac{\Omega^*(\mathbf{r})L(\mathbf{r}-\mathbf{r}')\Omega(\mathbf{r}')}{\Delta^2}\hat{\Psi}_g^\dagger(\mathbf{r})\hat{\Psi}_g(\mathbf{r})\rho_s(t)\hat{\Psi}_g^\dagger(\mathbf{r}')\hat{\Psi}_g(\mathbf{r}') + \text{H.c.}
\end{aligned}$$

where we have written $\rho_s \equiv \rho_{00}$.


[1] M. Greiner, O. Mandel, T. Esslinger, T. W. Hänsch, and I. Bloch, Nature (London) **415**, 39 (2002).

[2] T. Kinoshita, T. Wegner, and D. S. Weiss, Science **305**, 1125 (2004).

[3] C. D. Fertig, K. M. O'Hara, J. H. Huckans, S. L. Rolston, W. D. Phillips, and J. V. Porto, Phys. Rev. Lett. **94**, 120403 (2005).

[4] B. L. Tolra, K. M. O'Hara, J. H. Huckens, W. D. Phillips, S. L. Rolston, and J. V. Porto, Phys. Rev. Lett. **92**, 190401 (2004).

[5] B. Paredes, A. Widera, V. Murg, O. Mandel, S. Fölling, I. Cirac , G. V. Shlyapnikov, T. W. Hänsch, I. Bloch, Nature (London) **429**, 277 (2004).

[6] M. Greiner, C. A. Regal, and D. S. Jin, Phys. Rev. Lett. **94**, 070403 (2005).

[7] Jelena Stajic, J. N. Milstein, Qijin Chen, M. L. Chiofalo, M. J. Holland, and K. Levin, Phys. Rev. A **69**, 063610 (2004).

[8] T.-L. Ho, Phys. Rev. Lett. **87**, 060403 (2002).

[9] J. R. Abo-Shaeer, C. Raman, and W. Ketterle, Phys. Rev. Lett. **88**, 070409 (2002).

[10] J. J. Bollinger, W. M. Itano, D. J. Wineland, and D. J. Heinzen, Phys. Rev. A **54**, R4649 (1996).

[11] M. P. A. Fisher, B. P. Weichman, G. Grinstein, and D. S. FischerPhys. Rev. B **40**, 546 (1989).

[12] E. Schrödinger, Naturwiss. **23**, 807 (1935); **23**, 823 (1935); **23**, 844 (1935).

[13] W. H. Zurek, Phys. Today **44**, 10), 36 (1991).

[14] J. R. Friedman, V. Patel, W. Chen, S. K. Tolpygo, and J. E. Lukens, Nature (London) **60**, 43 (2000).

[15] M. Arndt, O. Nairz, J. Vos-Andreae, C. Keller, G. van der. Zouw, and A. Zeilinger, Nature (London) **401**, 680 (1999).
[16] C. Monroe, D. M. Meekhof, B. E. King, and D. J. Wineland, Science **272**, 1131 (1996).
[17] C. A. Sackett, D. Kielpinski, B. E. King, C. Langer, V. Meyer, C. J. Myatt, M. Rowe, Q. A. Turchette, W. M. Itano, D. J. Wineland, and C. Monroe, Nature (London) **404**, 256 (2000).
[18] J. R. Friedman, M. P. Sarachik, J. Tejada, and R. Ziolo, Phys. Rev. Lett. **76**, 3830 (1996).
[19] R. Rouse, S. Han, and J. E. Lukens, Phys. Rev. Lett. **75**, 1614 (1995).
[20] P. Silvestrini, V. G. Palmieri, B. Ruggiero, and M. Russo, Phys. Rev. Lett. **79**, 3046 (1997).
[21] Y. Nakamura, Y. A. Pashkin, and J. S. Tsai, Nature (London) **398**, 786 (1999).
[22] T. J. Osborne and M. A. Nielsen, Phys. Rev. A **66**, 032110 (2002).
[23] M. C. Arnesen, S. Bose, and V. Vedral, Phys. Rev. Lett. **87**, 017901 (2001).
[24] M. H. Anderson, J. R. Ensher, M. R. Matthews, C. E. Wieman, and E. A. Cornell, Science **269**, 198 (1995).
[25] C. C. Bradley, C. A. Sackett, J. J. Tollett, and R. G. Hulet, Phys. Rev. Lett. **75**, 1687 (1995).
[26] K. B. Davis, M.-O. Mewes, M. R. Andrews, N. J. van Druten, D. S. Durfee, D. M. Kurn, and W. Ketterle, Phys. Rev. Lett. **75**, 3969 (1995).
[27] F. Dalfovo, S. Giogini, L. P. Pitaevskii, and S. Stringari, Rev. Mod. Phys. **71**, 463 (1999).
[28] A. J. Leggett, Rev. Mod. Phys. **73**, 307 (2001).
[29] A. P. Hines, R. H. McKenzie, and G. J. Milburn, Phys. Rev. A **67**, 013609 (2003).
[30] S. Raghavan, A. Smerzi, and V. M. Kenkre, Phys. Rev. A **60**, R1787 (1999).
[31] K. W. Mahmud, H. Perry, and W. P. Reinhardt, J. Phys. B **36**, L265 (2003).
[32] A. Micheli, D. Jaksch, J. I. Cirac, and P. Zoller, Phys. Rev. A **67**, 013607 (2003).
[33] A. Sørenson, L.-M. Duan, J. I. Cirac and P. Zoller, Nature (London) **409**, 63 (2001).
[34] J. Higbie and D. M. Stamper-Kurn, Phys. Rev. A **69**, 053605 (2004).
[35] M. Greiner, O. Mandel, T. Esslinger, T. W. Hänsch, and I. Bloch, Nature (London) **415**, 39 (2002).
[36] J. I. Cirac, M. Lewenstein, K. Mølmer, and P. Zoller, Phys. Rev. A **57**, 1208 (1998).
[37] T.-L Ho and C. V. Ciobanu, J. Low Temp. Phys. **135**, 257 (2004).
[38] A. Smerzi, S. Fantoni, S. Giovanazzi, and S. R. Shenoy, Phys. Rev. Lett. **79**, 4950 (1997).
[39] S. Raghavan, A. Smerzi, S. Fantoni, and S. R. Shenoy, Phys. Rev. A **59**, 620 (1999).
[40] H. Feshbach, *Theoretical Nuclear Physics* (Wiley, New York, 1992).
[41] S. J. J. M. F. Kokkelmans, J. N. Milstein, M. L. Chiofalo, R. Walser, and M. J. Holland, Phys. Rev. A **65**, 053617 (2002).
[42] D. A. R. Dalvit, J. Dziarmaga, and W. H. Zurek, Phys. Rev. A **62**, 013607 (2000).
[43] P. J. Y. Louis, P. M. R. Brydon, and C. M. Savage, Phys. Rev. A **64**, 053613 (2001).
[44] G. Lenz, P. Meystre, and E. M. Wright, Phys. Rev. A **50**, 1681 (1994).
[45] Y. Castin and K. Mølmer, Phys. Rev. A **51**, R3426 (1995).
[46] W. Zhang, Phys. Lett. A **176**, 225 (1993).
[47] G. J. Milburn, J. Corney, E. M. Wright, and D. F. Walls, Phys. Rev. A **55**, 4318 (1997).
[48] J. K. Chin, J. M. Vogels, and W. Ketterle, Phys. Rev. Lett. **90**, 160405 (2003).
[49] Yu. Kagan, A. E. Muryshev and G. V. Shlyapnikov, Phys. Rev. Lett. **81**, 933 (1997).
[50] P. Meystre, *Atom Optics* (Springer-Verlag, New York, 2001).
[51] D. A. R. Dalvit, J. Dziarmaga, and R. Onofrio, Phys. Rev. A **65**, 033620 (2002).
[52] W. Zhang and D. F. Walls, Phys. Rev. A **49**, 3799 (1994).
[53] R. H. Dicke, Phys. Rev. **93**, 99 (1954).
[54] A. Imamoglu, M. Lewenstein, and L. You, Phys. Rev. Lett. **78**, 2511 (1997).
[55] J. A. Dunningham and K. Burnett, Phys. Rev. A **70**, 033601 (2004).